(4)

University of Washington

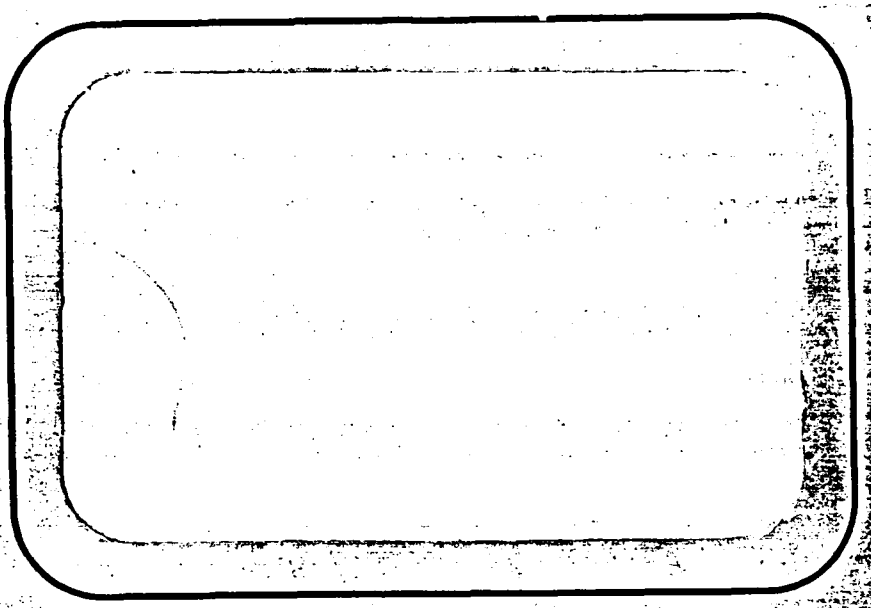

Aerospace and Energetics Research Program

(4)

INVESTIGATION OF SUPERDETONATIVE RAM ACCELERATOR DRIVE MODES

A.P. Bruckner and A. Hertzberg

Final Report
ONR Contract No. N00014-88-K-0565
1 July 1988 - 30 June 1989

Aerospace and Energetics Research Program
University of Washington, FL-10
Seattle, WA 98195

Prepared for:

Office of Naval Research
Arlington, VA

15 December 1989

SECURITY CLASSIFICATION OF THIS PAGE

REPORT DOCUMENTATION PAGE

1a. REPORT SECURITY CLASSIFICATION Unclassified	1b. RESTRICTIVE MARKINGS None
2a. SECURITY CLASSIFICATION AUTHORITY	3. DISTRIBUTION/AVAILABILITY OF REPORT Distribution Unlimited
2b. DECLASSIFICATION/DOWNGRADING SCHEDULE	
4. PERFORMING ORGANIZATION REPORT NUMBER(S)	5. MONITORING ORGANIZATION REPORT NUMBER(S)
6a. NAME OF PERFORMING ORGANIZATION Aerospace & Energetics Research Program, FL-10 6b. OFFICE SYMBOL (If applicable) 12104	7a. NAME OF MONITORING ORGANIZATION Office of Naval Research U of W Resident Representative N63374
6c. ADDRESS (City, State, and ZIP Code) Grant & Contract Services, JM-24 University of Washington Seattle, WA 98195	7b. ADDRESS (City, State, and ZIP Code) University of Washington 1107 NE 45th St, Univ Dist Bldg Rm 410 Seattle, WA 98105-4631
8a. NAME OF FUNDING/SPONSORING ORGANIZATION Office of Naval Research 8b. OFFICE SYMBOL (If applicable) N00014	9. PROCUREMENT INSTRUMENT IDENTIFICATION NUMBER N00014-88-K-0565
8c. ADDRESS (City, State, and ZIP Code) Propulsion & Energetics Division, code 1132P 800 No. Quincy Street Arlington, Virginia 22217-5000	10. SOURCE OF FUNDING NUMBERS PROGRAM ELEMENT NO. / PROJECT NO. 1132P / TASK NO. / WORK UNIT ACCESSION NO.

11. TITLE (Include Security Classification)

"Investigation of Superdetonative Ram Accelerator Drive Modes"

12. PERSONAL AUTHOR(S)
BRUCKNER, A.P. and HERTZBERG, A.

13a. TYPE OF REPORT	13b. TIME COVERED	14. DATE OF REPORT (Year, Month, Day)	15. PAGE COUNT
final technical report	FROM 7/1/88 TO 6/30/89	1989 December 15	61

16. SUPPLEMENTARY NOTATION
n/a

17. COSATI CODES		
FIELD	GROUP	SUB-GROUP

18. SUBJECT TERMS (Continue on reverse if necessary and identify by block number)
Ram Accelerator; Hypervelocity Launcher; Chemical Propulsion; Shock-Induced Combustion

19. ABSTRACT (Continue on reverse if necessary and identify by block number)

This report presents the results of experimental and theoretical investigations of high velocity modes of the ram accelerator, a ramjet-in-tube projectile accelerator whose principle of operation is similar to that of a supersonic airbreathing ramjet. The projectile resembles the centerbody of a ramjet and travels through a stationary tube filled with a premixed gaseous fuel and oxidizer mixture. The tube acts as the outer cowling of the ramjet, and the combustion process travels with the projectile, generating a pressure field which produces forward thrust on the projectile. Different modes of combustion have been explored for accelerating projectiles of nearly identical geometry. Subsonic, thermally choked combustion theoretically allows a projectile to be accelerated to the Chapman-Jouguet (C-J) detonation speed of a particular gas mixture. In the superdetonative regime the same projectile is accelerated while always traveling faster than the detonation speed, and in the transdetonative regime (85-115% of detonation speed) the same projectile may transit smoothly from a subsonic to a superdetonative combustion mode. This report examines operation in these three regimes of flow up to velocities approaching 2500 m/s in a 12.2 m long, 38 mm bore ram accelerator, using projectiles of 45-75 gm mass. Experimental evidence of acceleration in the transdetonative and superdetonative regimes is introduced. Also presented are the results of a computational fluid dynamics (CFD) code being developed for studying the flow, combustion, and performance of the ram accelerator, particularly in the superdetonative regime. The code solves the 2D, axisymmetric Euler equations with coupled chemical nonequilibrium processes, using a shock-capturing technique, and gives theoretical results which show that efficient acceleration of projectiles is possible through velocities as high as 9 km/sec.

20. DISTRIBUTION/AVAILABILITY OF ABSTRACT	21. ABSTRACT SECURITY CLASSIFICATION	
☐ UNCLASSIFIED/UNLIMITED ☒ SAME AS RPT. ☐ DTIC USERS	Unclassified	
22a. NAME OF RESPONSIBLE INDIVIDUAL Donald W. Allen	22b. TELEPHONE (Include Area Code) (206) 543-4043	22c. OFFICE SYMBOL 12104

DD FORM 1473, 84 MAR 83 APR edition may be used until exhausted. All other editions are obsolete.

SECURITY CLASSIFICATION OF THIS PAGE
Unclassified

ABSTRACT

This report presents the results of experimental and theoretical investigations of high velocity modes of the ram accelerator, a ramjet-in-tube projectile accelerator whose principle of operation is similar to that of a supersonic airbreathing ramjet. The projectile resembles the centerbody of a ramjet and travels through a stationary tube filled with a premixed gaseous fuel and oxidizer mixture. The tube acts as the outer cowling of the ramjet, and the combustion process travels with the projectile, generating a pressure field which produces forward thrust on the projectile. Different modes of combustion have been explored for accelerating projectiles of nearly identical geometry. Subsonic, thermally choked combustion theoretically allows a projectile to be accelerated to the Chapman-Jouguet (C-J) detonation speed of a particular gas mixture. In the superdetonative regime the same projectile is accelerated while always traveling faster than the detonation speed, and in the transdetonative regime (85-115% of detonation speed) the same projectile may transit smoothly from a subsonic to a superdetonative combustion mode. This report examines operation in these three regimes of flow up to velocities approaching 2500 m/s in a 12.2 m long, 38 mm bore ram accelerator, using projectiles of 45-75 gm mass. Experimental evidence of acceleration in the transdetonative and superdetonative regimes is introduced. Also presented are the results of a computational fluid dynamics (CFD) code being developed for studying the flow, combustion, and performance of the ram accelerator, particularly in the superdetonative regime. The code solves the 2D, axisymmetric Euler equations with coupled chemical nonequilibrium processes, using a shock-capturing technique, and gives theoretical results which show that efficient acceleration of projectiles is possible through velocities as high as 9 km/sec.

PREFACE

This program was conducted during the period 1 July 1988 to 30 June 1989 by the Aerospace and Energetics Research Program, University of Washington, Seattle, WA 98195, under Contract No. N00014-88-K-0565 from the Office of Naval Research, 800 North Quincy St., Arlington, VA 22217-5000. Dr. Richard S. Miller managed the program for ONR.

The authors are deeply indebted to Alan Kull, Ed Burnham, Carl Knowlen, Peter Kaloupis, Gilbert Chew and Erik Christofferson for their assistance in performing the experiments, to Shaye Yungster for the CFD computations, and to Bill Lowe, Malcolm Saynor, and Dennis Peterson for their skillful fabrication of the projectiles.

TABLE OF CONTENTS

I. INTRODUCTION

At the University of Washington experimental and theoretical research is being carried out on the acceleration of projectiles to ultrahigh velocities using a ramjet-in-tube concept called the "ram accelerator." [1-10] The projectile resembles the centerbody of a conventional ramjet and is accelerated by combustion through a stationary tube filled with a reactive gas mixture (see Figs. 1 and 2). There is no propellant on board the projectile. The pressure, composition, chemical energy density, and speed of sound of the mixture can be controlled to optimize the ballistic efficiency (defined here as the ratio of the rate of change of kinetic energy of the projectile to the rate of expenditure of chemical energy). The concept is scalable over a wide range of projectile masses and has the potential for a number of applications, such as hypervelocity impact studies,[11] direct launch to orbit of acceleration-insensitive payloads,[12,13] hypersonic testing, and both tactical and strategic military applications, such as armor penetration and the Strategic Defense Initiative.

In view of the broad application possibilities of this concept, which reflect favorably on the capabilities of the Armed Services, a program of theoretical study was initiated by the authors in September 1983. The novel nature of this concept suggested that a proof-of-concept experiment be undertaken and a facility was built in 1985, with Air Force and University funding, to carry out the necessary experiments. This unique facility was not only designed to study the proof of concept but also to develop a practical methodology of operation. Experimental proof of concept was demonstrated in June 1986, and was followed by verification of scaling laws with relation to velocity, fill pressure, mass, acceleration, and efficiency in the velocity range of 690-2500 m/sec.[1-8] The agreement between a simplified thermodynamic model and the actual experimental results was excellent. The learning process involved in this exploratory program led to the formulation of additional modes of operation and capabilities which would expand the usefulness of the ram accelerator to the armed services in the realm of tactical and strategic capabilities.

Several modes of ram accelerator operation, which span the velocity range of 0.7-12 km/sec, have been proposed by the authors.[2,4,5] These include, among others, a thermally choked subsonic combustion mode, shown in Fig. 1, and two superdetonative modes, one of which is shown in Fig. 2. (Both are described in more detail in Section II). The thermally choked subsonic combustion mode has been extensively studied experimentally by the authors and their colleagues,[1-8] and has attained velocities in excess of 2500 m/sec with 70 gm projectiles in a 12.2 m long 38 mm bore accelerator tube. In the superdetonative modes the

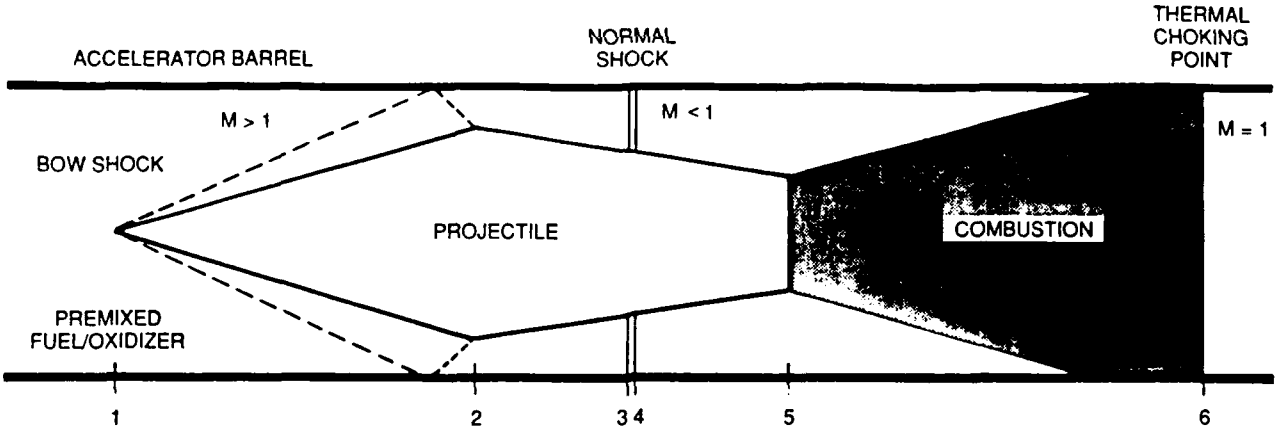

Fig. 1 Subsonic combustion thermally choked ram accelerator mode.

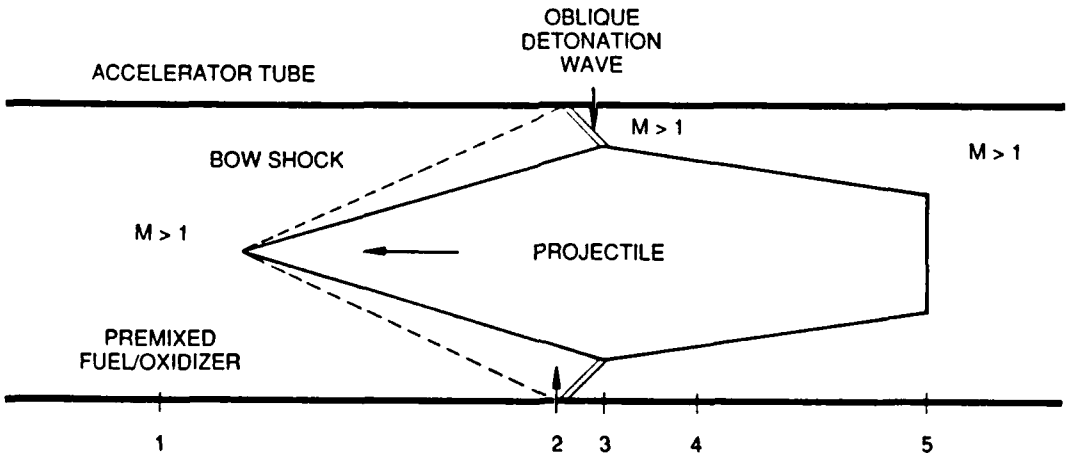

Fig. 2 Superdetonative ram accelerator mode.

gasdynamic principles of the ram accelerator are similar to those of the Oblique Detonation Wave Engine (ODWE),[14,15] which has been proposed as an alternative to the scramjet engine for propelling hypersonic airbreathing vehicles such as the National Aerospace Plane (NASP).

To operate in the superdetonative modes the projectile must fly at speeds above the local Chapman-Jouguet (C-J) detonation speed of the gas mixture. In operation the combustion occurs either immediately at the reflected shock (oblique detonation wave) or somewhat downstream (shock induced deflagration). Early theoretical studies by the authors and their colleagues indicated that by judicious selection of gas mixtures the ram accelerator will, in principle, operate superdetonatively in the velocity range 2-12 km/sec.[4] The purpose of the investigation reported here was to attempt to experimentally verify superdetonative operation of the ram accelerator and to develop improved computational models with which to predict the performance of the device over a broad range of operational parameters.

Both these goals have been attained and are presented in this report. Experimental confirmation of superdetonative ram accelerator operation in the velocity range 2000-2500 m/sec in hydrocarbon-based propellant mixtures has been achieved and a new CFD approach has been successfully implemented. In addition, it has been experimentally observed that while operating in the subdetonative regime, at velocities greater than 85% of C-J speed, the projectile often accelerates at a higher rate than is predicted by theoretical models for subsonic, thermally choked combustion. Further experiments have shown that in this "transdetonative" regime (85-115% of C-J speed), the projectile can accelerate smoothly from subdetonative to superdetonative speeds in a single gas mixture. These results are also discussed in this report.

Section II of the report describes the various ram accelerator propulsion modes and their general capabilities in greater detail. This is followed in Section III by a description of the experimental facility. Section IV is devoted to a discussion of the experimental results and Section V presents a description of the CFD modelling of the superdetonative acceleration process and the results of computations for a number of cases of interest.

II. RAM ACCELERATOR DRIVE MODES

The subsonic combustion, thermally choked ram accelerator drive mode is shown in Fig. 1. The projectile is injected into the accelerator tube by a conventional powder or gas gun. The gas mixture in the accelerator tube is chosen so that the projectile Mach number is initially in the range of 2.5-3. The cone angle of the nose is chosen such that the oblique shock system in the diffuser does not initiate combustion. A normal shock is located downstream of the projectile throat; this shock is also not strong enough to initiate combustion. The combustion zone is established behind the projectile and the choking of the flow by the heat release stabilizes the normal shock on the projectile. Combustion is initiated by an external ignitor.

Above velocities of approximately 2.7-3 km/sec subsonic combustion can no longer maintain a sufficiently high ballistic efficiency, even with hydrogen-based propellant mixtures. To continue efficient acceleration to higher velocities, alternative concepts, which employ shock waves to generate combustion, have been proposed by the authors.[2,4,5] One of these is illustrated in Fig. 2. The projectile velocity must exceed the Chapman-Jouguet (C-J) detonation speed of the propellant gas, hence this mode is referred to as "superdetonative" propulsion. A transition to the superdetonative mode can be achieved through an abrupt change of propellant mixture in the accelerator tube at the appropriate location, using a thin diaphragm to separate the mixtures. If the second mixture is tailored to have a detonation speed sufficiently below the speed of the projectile, transition to the superdetonative mode occurs automatically. The cone angle of the nose, the projectile velocity, and the speed of sound of the mixture are tuned so that the initial conical shock does not initiate combustion, but the first or second reflected shock does.

In principle, the superdetonative ram accelerator mode can attain velocities up to 12 km/sec, using hydrogen-oxygen propellant mixtures diluted with hydrogen or helium.[4] Estimates of heat transfer rates to the projectile, however, indicate that in-tube aerodynamic heating and ablation become severe at velocities exceeding 6 km/sec, depending on the specific propellant composition employed. The heat transfer to the projectile can be greatly reduced by laying down a cylindrical core of pure hydrogen, surrounded by the propellant mixture.[16] This approach, in principle, allows operation of the ram accelerator to velocities in excess of 10 km/sec.

In principle, the modes of propulsion discussed above are scalable from fractions of a kilogram to hundreds of kilograms and can be combined to span the entire velocity range from ~0.7 km/sec to ~10 km/sec. Transition from the subsonic combustion mode to the

superdetonative mode can be achieved at a velocity as low as 2 km/sec by judicious choice of a low detonation speed gas mixture. In each mode the heat and pressure pulses travel with the projectile, distributing the heat over the entire length of the launch tube. Consequently, the temperature rise of the tube is relatively small and very little tube wear is expected.

For the ram accelerator, specific impulse does not have its usual meaning, since no fuel or oxidizer is carried onboard the projectile. Rather, the performance of the device can be characterized by two main parameters: thrust pressure ratio and ballistic efficiency.[2] The thrust pressure ratio is the net average drive pressure on the projectile (the thrust divided by the maximum projectile cross-sectional area) divided by the maximum cycle pressure. This ratio is an important performance parameter because it provides a measure of the device's launch capability versus the maximum pressure the projectile and launch tube must survive.

III. EXPERIMENTAL RAM ACCELERATOR FACILITY

The principal components of the University of Washington ram accelerator facility, illustrated in Fig. 3, are the 38 mm bore single-stage light gas gun, ram accelerator section, final dump tank and projectile decelerator. Associated subsystems are the gas handling system, instrumentation, and data acquisition system. In what follows, these and related components, as well as the projectile design, are described in detail.

Light Gas Gun

The single-stage light gas gun is of conventional design. The high pressure driver, designed for up to 400 atm load pressure, consists of a cylindrical flanged tube machined from heat-treated 4142 alloy steel and has the following principal dimensions: 10 cm I.D. x 20 cm O.D. x 1.8 m long. A double diaphragm section connects the driver section to the adjacent launch tube. The diaphragms are made from 1100-0 (dead soft) aluminum sheets of appropriate thickness coined with two knife edge scores, 90° apart. The interdiaphragm space is pressurized to about two-thirds of the breaking pressure of the diaphragm. The driver is filled to about four-thirds of the breaking pressure. Thus, when the gas in the interdiaphragm space is released, both diaphragms rupture.

The launch tube section is composed of three 2.44 m long, 38 mm bore, 76 mm O.D. tubes made of heat-treated 4150 alloy steel. Each tube section has a double 0-ring seal at both ends and the tube joints are held together by threaded collars. The tubes rest on ball bearing support stands, which allow axial movement of each tube for periodic maintenance and inspection. At the end of the last launch tube, three pairs of instrumentation ports have been tapped into the sidewall. These are diametrically opposed and spaced at 15.2 cm intervals. One set of adjacent instrumentation ports is equipped with electromagnetic transducers which detect the passage of a magnet on the projectile. The signal from the upstream transducer is used to trigger the data acquisition system. The signals from both transducers together provide velocity data. The unused ports are closed off with blank plugs.

The light gas gun is capable of accelerating the sabot and projectile combination (typical combined mass of 60-100 gm) to speeds up to approximately 1350 m/sec. The end of the launch tube is connected to a 1.52 m long perforated wall tube, having similar internal and external diameters, that passes through an evacuated cylindrical tank, 1.07 m I.D. by 0.91 m

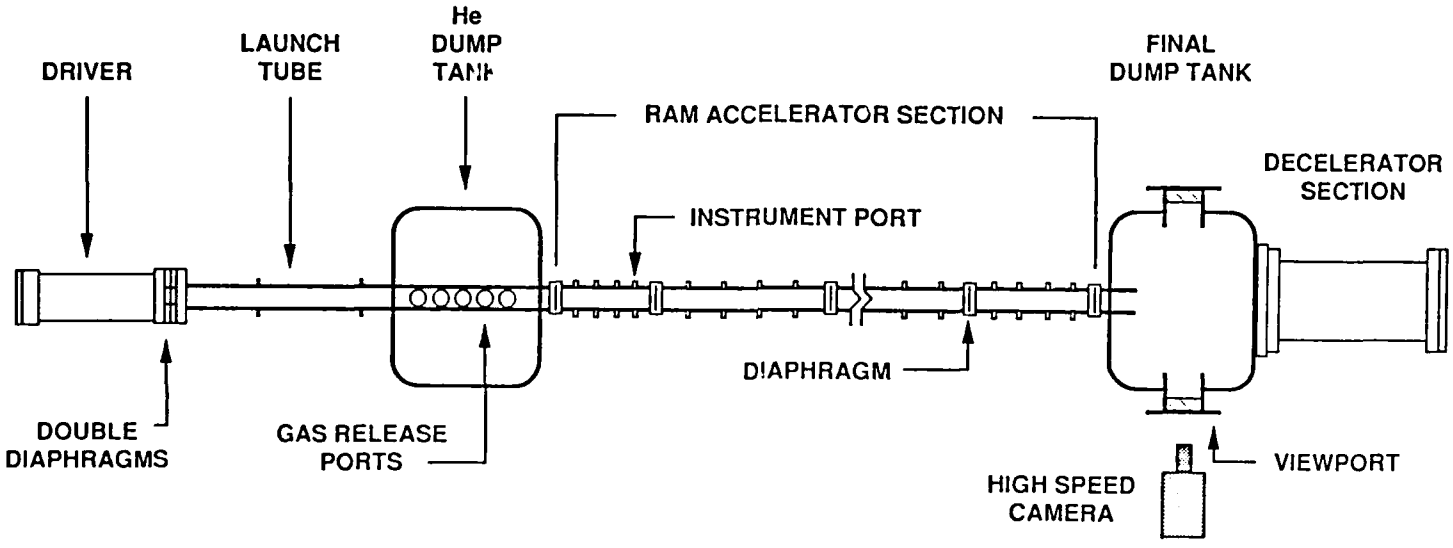

Fig. 3 Ram accelerator test facility.

long, which serves as a dump for the helium driver gas. This tank has 0-ring seal collars on both ends to allow axial movement of the tube. A second dump tank of similar dimensions is connected to the first one by a 25 cm dia. tube to provide a larger dump volume.

Ram Accelerator

The 12.2 m long ram accelerator section consists of seven tubes made from heat-treated 4150 steel alloy. These tubes have a 38 mm bore and a 100 mm O.D. Four of these tubes are 1.22 m long apiece and have four pairs of diametrically opposed instrumentation ports tapped at 30.5 cm intervals. The other three tubes are 2.44 m long apiece and also have four pairs of diametrically opposed instrumentation ports but located at 61 cm intervals. Two of these tubes feature dual pairs of instrumentation ports, spaced at 90 degrees circumferentially, at the two ends. The short and long tubes are arranged in alternating fashion. A total of 60 instrumentation ports are available with which to observe the progress of the projectile. Typically, the ports are instrumented with Kistler and PCB quartz pressure transducers, custom-made electromagnetic velocity transducers, fiber-optic light emission probes, and the gas lines that are used to evacuate and then fill the various segments of the ram accelerator with the desired combustible gas mixtures. Unused ports are blanked off with solid plugs. Thin mylar diaphragms close off each end of the ram accelerator and are also used to separate the segments of the tube which are filled with different propellant mixtures. The ram accelerator is designed to operate at propellant fill pressures up to 50 atm, which would result in peak drive pressures in excess of 50,000 psi on the projectile when operating in the superdetonative mode. To date the maximum fill pressure used has been 37 atm.

Final Dump Tank

When the accelerated projectile leaves the ram accelerator it travels through the final mylar diaphragm into a drift tube, 0.76 m long x 38 mm I.D. x 76 mm O.D., and thence into the final evacuated dump tank, 1.22 m O.D. x 2.44 m long, where it flies free. A pair of diametrically opposed 25 cm dia. viewing portholes provide a means to observe the projectile in flight. A high speed spark shadowgraph photography system (exposure time approximately 300 ns) is used to photograph the projectile as it flies through the final dump tank.

Projectile Decelerator

The decelerator serves to bring the spent projectile to a stop. It consists of a 1.83 m long steel tube with 17.8 cm I.D. and 35.6 cm O.D. and has a 7.6 cm thick end plate. The tube is separated from the final dump tank by a thin aluminum sheet which has perforations on its periphery to equalize the pressure between the two volumes. This sheet acts as a witness plate and serves to initiate projectile breakup. The decelerator tube is filled with tightly packed carpet remnants and steel lathe turnings which bring the projectile fragments to rest.

Gas Handling System

Commercial bottled helium at a pressure of 160 atm provides the gun gas supply. To attain higher pressures, a diaphragm pump capable of reaching 400 atm is used. Two vacuum pumps serve to evacuate the launch tube and the three dump tanks. The fuel, oxidizer, and diluent gases are sent through filters and sonic orifices to a gas mixer (carburetor) and then on to the ram accelerator section. The gas mixer consists of a cylindrical vessel, 5.0 cm inside diameter 75 cm long, having a multitude of offset baffles which promote turbulence and hence good mixing. The ram accelerator can be filled with up to five different gas mixtures. The desired mixture ratio in each segment is obtained by adjusting the feed pressures of the individual constituents. This mixing system has been calibrated and is regularly checked by having mixture samples analyzed by a local testing laboratory. Two armored bunkers are used for the protection of personnel and high pressure gas cylinders. The personnel bunker houses the pressure, vacuum and gas mixing control panels, the high pressure pump, the two vacuum pumps and the data acquisition system.

Data Acquisition System

A 28-channel LeCroy Research Systems Corp. data acquisition system (DAS) is used. All the pressure transducer, electromagnetic transducer and fiber-optic signals travel through coaxial cables to LeCroy Model 8210 10-bit and 6810 12-bit transient digitizers. Some of the inputs are separately multiplexed, effectively permitting up to 50 different sets of data to be recorded. The digitizers use track and hold circuits, capable of handling four analog inputs per module. The analog input signals are digitized and stored in buffer memory modules. The data are read out through the memory control circuit and each of the four channels can be separately addressed. The seven modules, along with a 32-channel data logger and CAMAC to

GPIB interface, are contained within a CAMAC crate which contains the power supply. The CAMAC to GPIB interface connects to an IBM PC-compatible microcomputer. A LeCroy Wave-Form Catalyst® software program is used to manipulate and display the data.

Projectile Configuration

The basic projectile geometry used in in the majority of the experimental studies to date is illustrated in Fig. 4. The projectile is fabricated from magnesium in two pieces: the nose cone and the body with integral fins. Both nose and body are hollow. For ease of machining, the body has an octagonal cross-section with fins at four opposed vertices. The purpose of the fins is to center the projectile in the tube. The fins and body are integral to assure survival of accelerations exceeding 40,000 g's. The truncated base of the projectile acts as a flame holding dump combustor for the thermally choked mode of operation. The nose cone is threaded into the body. At this joint is sandwiched a thin annular disk of flexible magnetic material. A second magnet is installed inside the projectile at its base. These magnets interact with the electromagnetic transducers, providing time of flight data from which the velocity of the projectile can be determined.

Two variations of the basic projectile configuration have been experimented with extensively and are referred to in Fig. 4 as type A and type B. The differences between the two projectile geometries used lie in the angle of the nose (10° and 12.5°) and the length of the body (71 mm and 84 mm). The longer body is used with the 10° nose. The maximum diameter of the projectile is 28.9 mm, which results in a diffuser area ratio of 2.37 in the 38 mm bore tube. The masses of the projectiles used have been in the range of 45 to 70 gm, depending on the external and internal configurations. The lexan launching sabot has a mass of 13 gm.

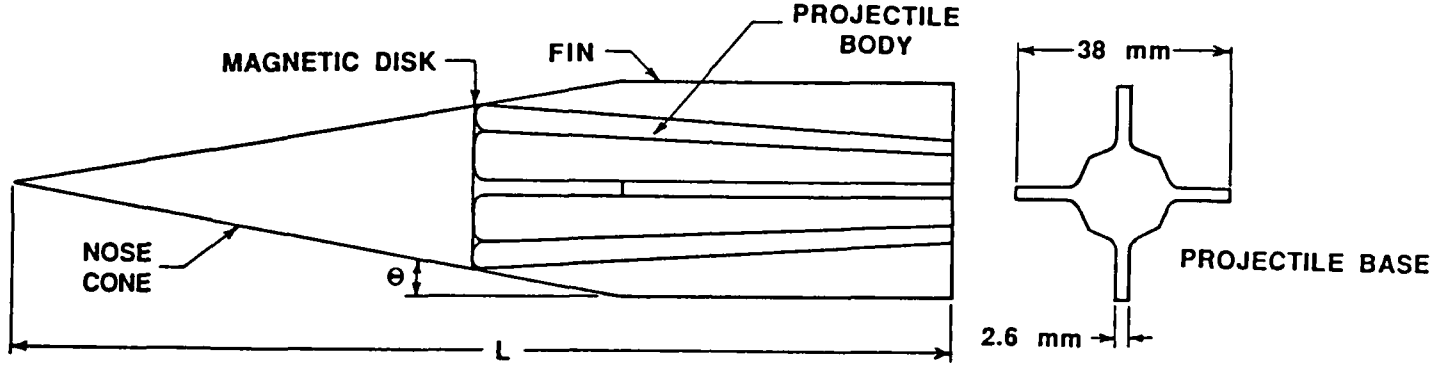

PROJECTILE

	TYPE A	TYPE B
L	138 mm	166 mm
θ	12.5°	10°

Fig. 4 Experimental projectile configuration.

IV. EXPERIMENTAL RESULTS

Thermally Choked Mode

Figure 5 illustrates typical transducer outputs obtained in the thermally choked combustion mode (subdetonative regime) in a tube segment containing $3.5CH_4 + 2O_2 + 6.5He$ at 25 atm. The projectile velocity and Mach number are 2020 m/s and 3.7, respectively. Time is measured from the instant of data acquisition system triggering, and pressure is measured in atmospheres. The pressure (middle) trace is typical of the thermally choked mode. The first pressure pulse is generated by the oblique shock system in the projectile diffuser section. There then follows a series of pulses which increase the pressure to a peak of approximately 430 atm, after which the pressure decays. The increase in pressure after the initial oblique shocks represents the normal shock, which is assumed to consist of a complex system of oblique and normal shocks similar to that observed in supersonic flow in long ducts.[17] The flow entering the combustion zone is subsonic. The decay in pressure following the peak is due to subsonic heat addition accelerating the flow to choking and the subsequent nonsteady expansion of the combustion products behind the choking point.

The upper trace in Fig. 5 displays the output of an electromagnetic transducer located at the same axial station as the pressure transducer. The zero crossing of the first signal identifies the passage by the sensor of the annular magnetic disk located at the projectile throat. The later zero crossing identifies the rear of the projectile. These signals provide convenient reference points from which the position of the shock system on the projectile can be determined. A profile of the projectile scaled to the local velocity is shown for reference.

The bottom trace in Fig. 5 shows the output from a fiber-optic probe located at the same station as the pressure and electromagnetic probes. The fiber-optic probes are used to examine the luminosity emitted as the projectile and combustion gases pass by the the probe. The primary radiation is assumed to be that from carbon particles generated by the fuel-rich combustion of methane and oxygen in the subsonic zone behind the projectile. The carbon particles emit blackbody radiation whose peak intensity occurs at the highest gas temperature.

As reported in earlier publications,[6,7] velocities up to 2500 m/s have been attained with the thermally choked mode of propulsion. Such performance has been achieved using a four-stage ram accelerator configuration, in which the accelerator tube is filled with successive

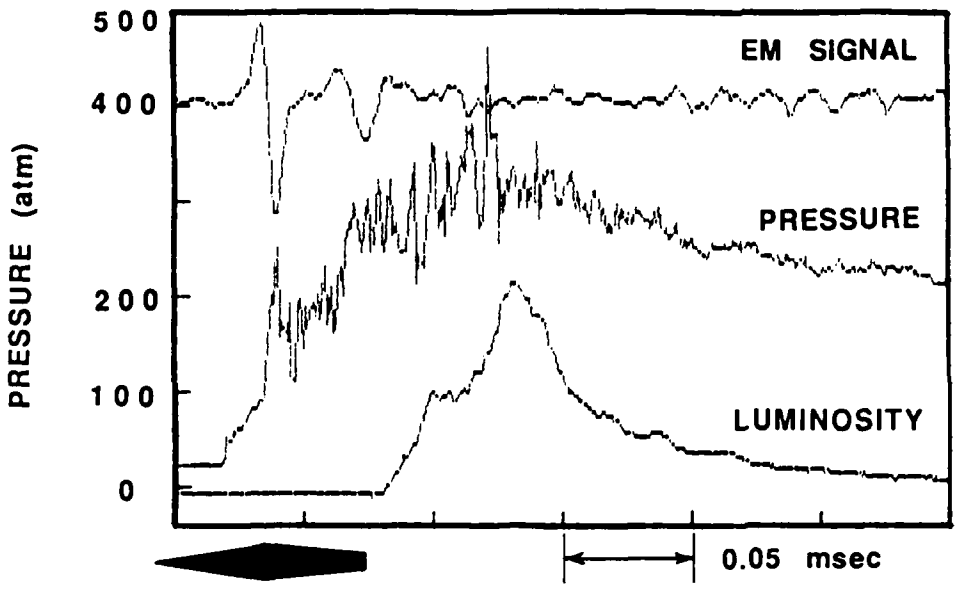

Fig. 5 Electromagnetic (EM), pressure and broadband luminosity signals in thermally choked ram accelerator operation. Propellant mixture $3.5CH_4 + 2O_2 + 6.5He$; fill pressure = 25 atm; U = 2020 m/s; M = 3.7; type B projectile.

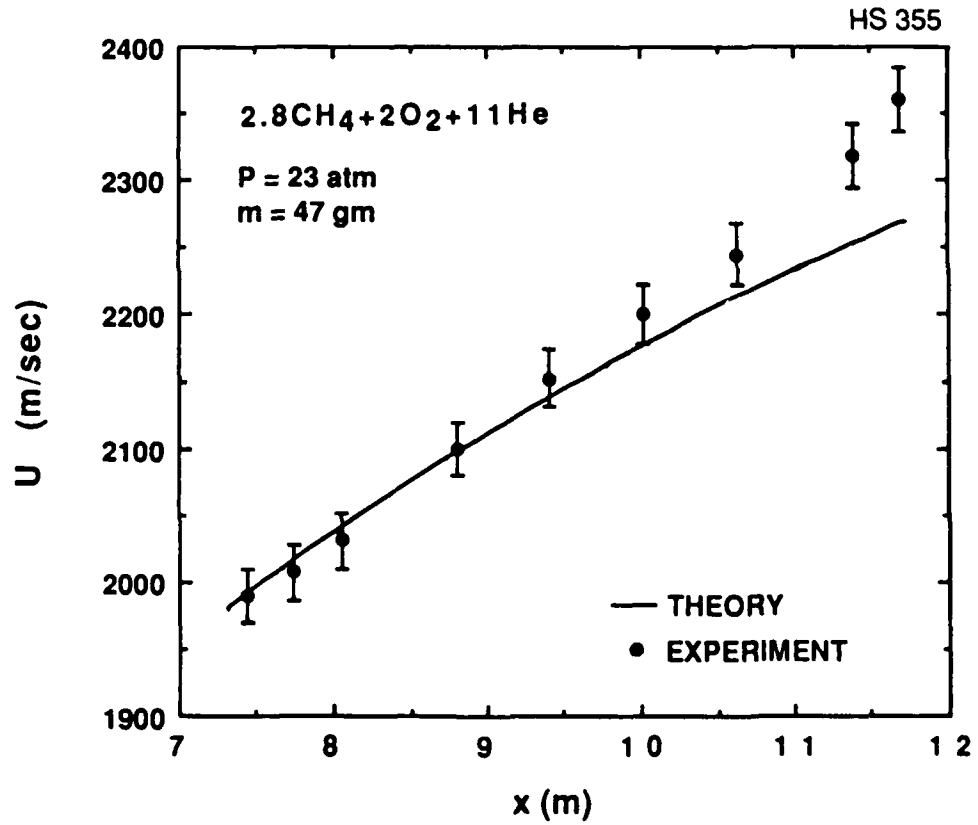

Fig. 6 Velocity profile in fourth stage of four-stage thermally choked ram accelerator. Type A projectile.

combustible gas mixtures whose acoustic speeds increase toward the muzzle. In this manner the projectile Mach number is kept within relatively narrow limits (~2.5-4.0) for maximum propulsive efficiency.

Transdetonative Regime

In the higher Mach number ranges of the thermally choked mode (typically 4-4.5), it has been observed from velocity vs. distance curves, such as the example shown in Fig. 6, that the experimentally measured velocities remain higher than theory predicts. The theoretical model, described in detail elsewhere,[2] is based on quasi-steady flow and predicts that the thrust on the projectile decreases as the projectile approaches the C-J detonation speed of the gas. This model further assumes that heat addition occurs only in the subsonic zone behind the projectile.

Accelerations much greater than that predicted by the thermally choked model are routinely observed when the projectiles attain velocities greater than 85% of the C-J speed of the propellant mixture. When close to the detonation velocity, the pressure waves on the rear half of the projectile often sweep forward through the projectile throat and unstart it. During this transient shock system activity the projectile velocity and acceleration increase abruptly before it unstarts. This behavior could be due to the initiation phase of a detonation wave at the rear of the projectile which gives it a boost before the wave completely washes over the projectile.

It was found that longer projectiles more closely approached the experimentally determined detonation speeds of the thermally choked mode propellant gases and in some cases actually accelerated through and above the C-J detonation velocity. It is postulated that the frequent discrepancy between theory and experiment in this transdetonative regime (85%-115% of C-J speed) may be explained by different modes of propulsion which do not require a thermal choking point at full tube area to stabilize the driving pressure wave system on the projectile. Heat addition is believed to occur at least partially on the projectile body. Credence is given to this hypothesis by data from the light fiber probes showing luminosity emanating from the rear half of the projectile at the high Mach number ranges of thermally choked operation.

Transdetonative propulsion suggests that it may be possible for projectiles to make a transition smoothly from thermally choked to superdetonative operation in one mixture. Figure 7 is a velocity versus distance plot of an experiment wherein the projectile entered a mixture of $4.5CH_4 + 2O_2 + 2He$ at a speed of 1300 m/sec (Mach 2.8) and accelerated to 2250 m/s (Mach 5.0). The experimentally determined detonation speed for this mixture was 2050 m/s. The projectile had a mass of 65 grams and the tube fill pressure was 25 atm. The solid line is the theoretical profile for the experiment. It shows good agreement with experiment up to about 85% of detonation speed, after which the experimental results outpace theory. The projectile accelerated through the detonation speed, exceeding it by 10% before exiting the tube. A characteristic of transdetonative operation, evident from Fig. 7, is that the acceleration increases dramatically with increasing velocity, a trend which is opposite to that observed during thermally choked operation.

A pressure and an electromagnetic transducer trace from the transdetonative regime are displayed in Fig. 8. These data were taken from the same experimental run plotted in Fig. 7. The projectile velocity and Mach number were 2150 m/s and 4.8, respectively. Although thermally choked, subdetonative theory predicts that the projectile loses thrust as it approaches the C-J speed, due to the shock wave moving back on the body, the figure clearly shows that the shock system is well-attached to the projectile body. Also because of the higher Mach number, the initial oblique shock system is narrower and much stronger than that of Fig. 5.

The details of propulsion in the transdetonative regime are the subject of ongoing research at the University of Washington. The exact mechanism by which heat is released during transdetonative operation is believed to be a "combined cycle" in which some heat is released on the projectile body and some in the recirculation zone behind it. The heat released on the body may come from partial shock-induced combustion (possibly supersonic), or the combustion may be making a transition from a subsonic to a supersonic (SCRAM) mode. Regardless of the mechanism, the existence of transdetonative propulsion may allow the projectile to be accelerated over a wide Mach number range -- from subdetonative to superdetonative -- in only one mixture, thus resulting in a simplification of the entire launch system.

Superdetonative Regime

In view of the excellent performance obtained in the transdetonative regime using a projectile shape designed for subdetonative operation, experiments were performed in which a high-speed projectile of the same geometry, operating in a thermally choked mode, abruptly

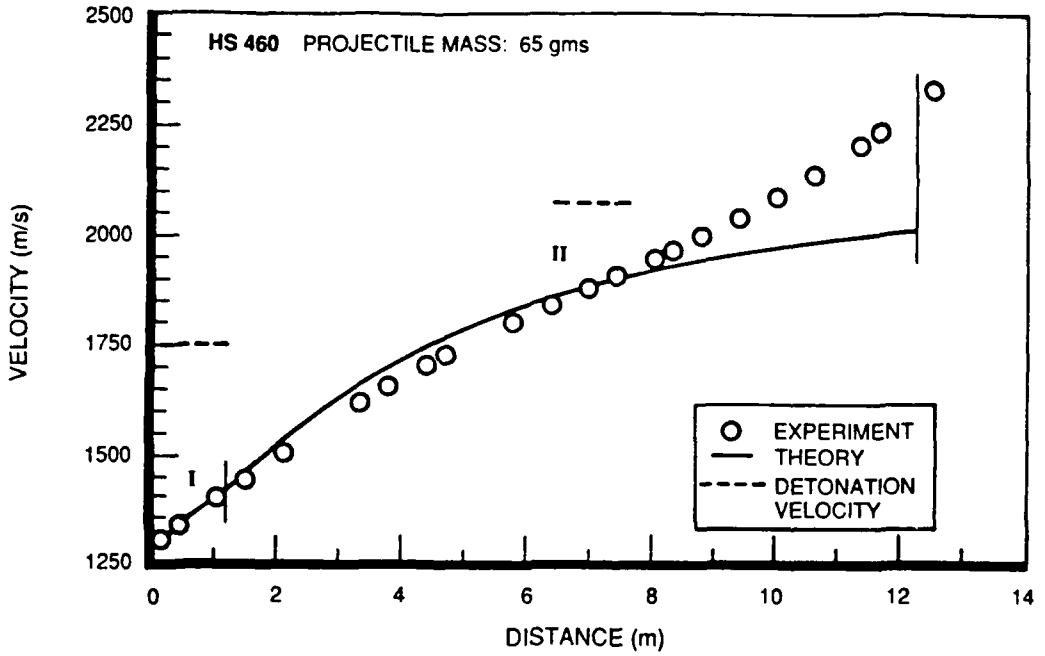

STAGE	MIX	SOUND SPEED	PRESSURE
I	2.6CH4 + 2O2 + 5.6N2	363 m/s	25 atm
II	4.5CH4 + 2O2 + 2He	448 m/s	25 atm

Fig. 7 Velocity profile in transdetonative ram accelerator operating regime.

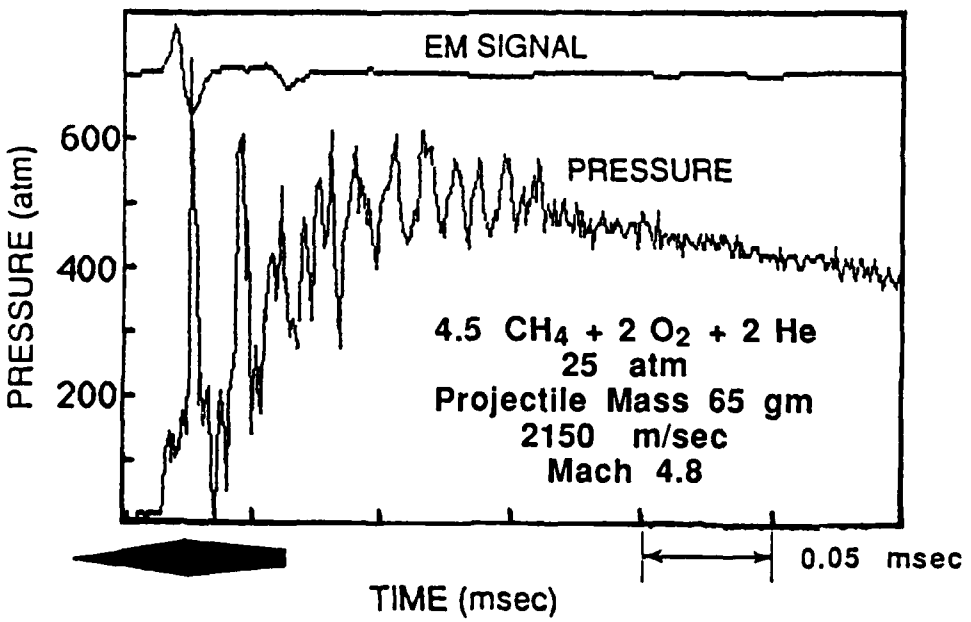

Fig. 8 Pressure and EM signatures in transdetonative ram accelerator operating regime.

entered a propellant mixture whose detonation speed was substantially lower than the projectile velocity. The projectile was observed to accelerate in this superdetonative regime.

In these experiments the first 8.5 m of tube were configured into a three-stage thermally choked ram accelerator to accelerate the 70 gm projectile to the 2000-2200 m/sec range, using methane-based propellant mixtures at nominal fill pressures of 25-30 atm, as described in Refs. 6-8. The last 3.66 m of the accelerator were filled with a mixture of $0.6C_2H_4 + 2O_2 + 3.3CO_2$ at 16 atm, which has an experimentally measured C-J detonation speed of 1650 m/sec (theoretical C-J speed is 1550 m/sec, based on equilibrium combustion). The projectile thus entered the final mixture at a velocity 20-30% higher than the C-J speed.

Figure 9 displays the outputs from a pressure transducer and an electromagnetic sensor at a point 0.5 m from the entrance to the last stage, where the projectile is operating in the superdetonative regime. The projectile velocity and Mach number are 2070 m/sec and 7.1, respectively. The pressure trace, typical of superdetonative operation, is completely different from that observed in the thermally choked mode (Fig. 5). In the present case there is an abrupt rise in pressure to 800 atm, i.e., a pressure ratio of 50, followed by a series of pressure pulses of decreasing amplitude. Eventually, a steady pressure plateau of 500 atm is reached.

Figure 10 displays the outputs from a pressure transducer and a light emission probe located 0.3 m ahead of the instruments in Fig. 9; the data in Fig. 10 are taken from the same experimental run as those in Fig. 9. The projectile velocity and Mach number are 2040 m/sec and 7.0, respectively. The features of the pressure trace are similar to those in Fig. 9. The light emission data are radically different from those in the thermally choked mode (Fig. 5). Along with the pressure traces, the light emission data suggest that combustion occurs mainly on the projectile body in contrast to the thermally choked mode, where all combustion activity occurs behind the projectile. The light emission behind the projectile in Fig. 10 may be a result of recombination or the formation of carbon particles. Currently, the exact combustion mode which drives the projectile in the superdetonative regime remains somewhat speculative, though recent CFD modeling indicates that shock-induced combustion may be the thrust-producing mechanism, as discussed in Section V of this report. Regardless of the exact mechanism, the gas pressure is seen to rise during the combustion process, indicating supersonic heat addition.

The velocity of the projectile down the tube was deduced from the distance-time history of the electromagnetic transducer signals. The data obtained were curve fit with the highest order polynomial (typically fifth- to seventh-order) that closely matched the experimental data

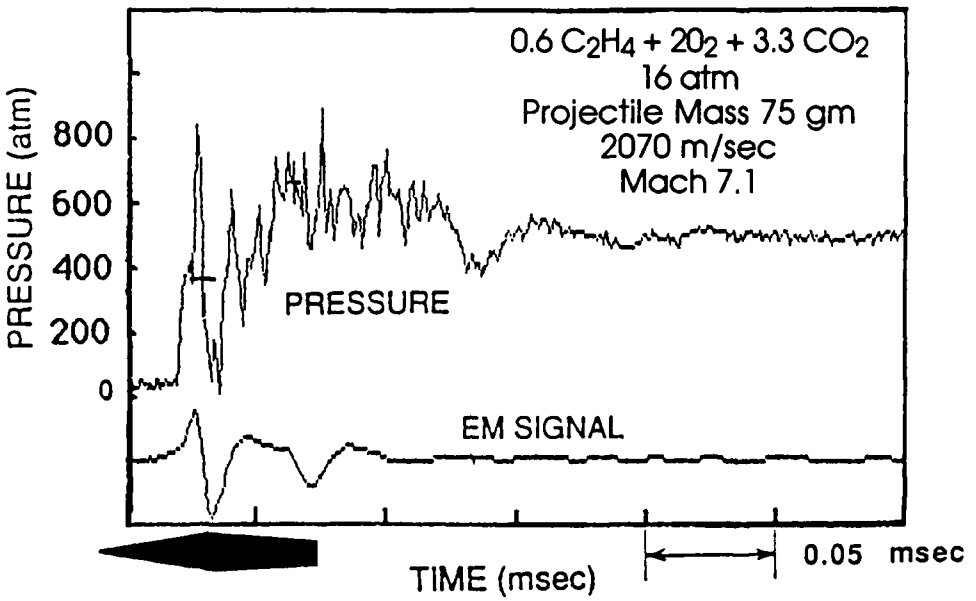

Fig. 9 Pressure and EM signatures in superdetonative ram accelerator operating regime.

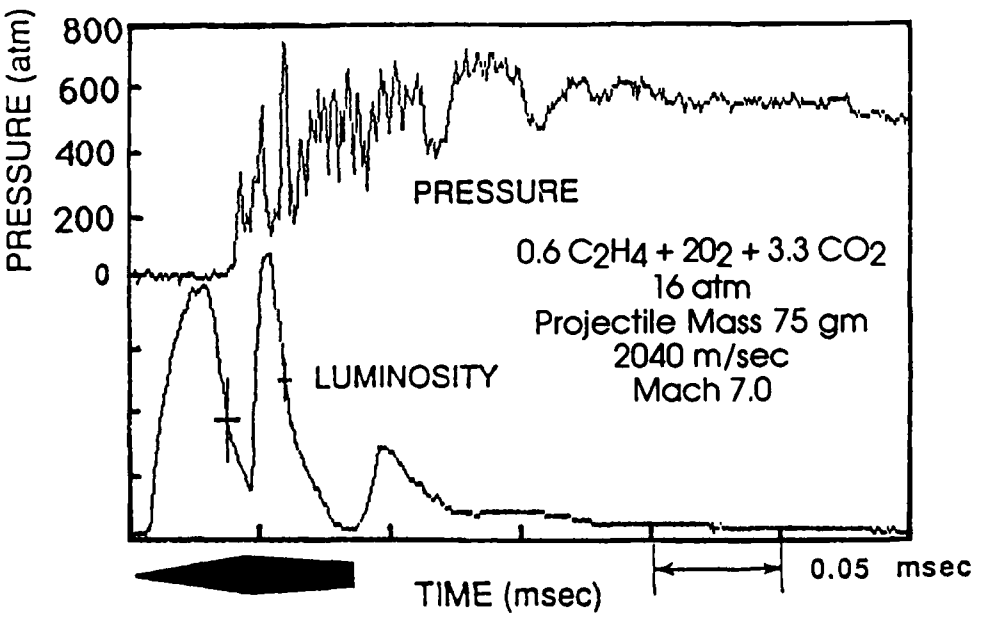

Fig. 10 Pressure and luminosity signatures in superdetonative ram accelerator operating regime.

without producing excessive oscillations in the distance-velocity history obtained by differentiation. Figure 11 shows the experimentally determined velocity as a function of distance in the entire ram accelerator, including the first three stages of thermally choked operation. The solid line is the theoretical velocity-distance curve for the corresponding experimental run. The theoretical curve is plotted only for the subdetonative, thermally choked combustion regime. A model of superdetonative operation is the subject of ongoing work. The operating conditions and the gas mixtures are noted in the figure. The short, dashed horizontal lines denote the C-J detonation speeds of the various gas mixtures. In this case superdetonative operation was observed over the velocity range 2180-2475 m/sec. The peak Mach number attained in the superdetonative regime was 8.4.

Although the experimentally attained velocities could not exceed ~2500 m/sec in the current facility, the high value of Mach number observed is significant. By using lower molecular weight fuels, such as hydrogen, propellant mixtures having higher acoustic and C-J detonation speeds can be formulated. With such mixtures projectile velocities in excess of 6 km/sec will be attainable without exceeding the Mach number regime in which superdetonative operation has already been achieved.

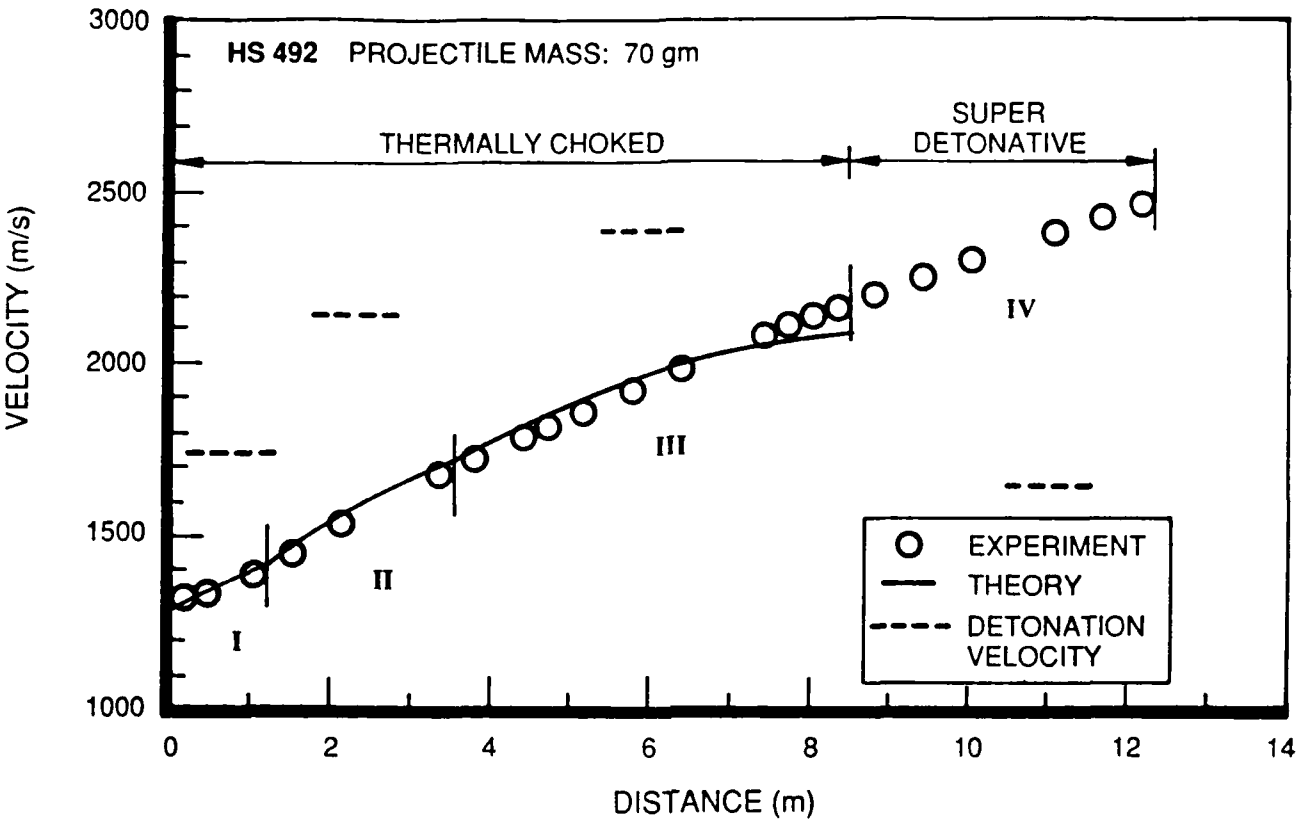

STAGE	MIX	SOUND SPEED	PRESSURE
I	2.6 CH_4 - 2 O_2 - 5.6 N_2	363 (m/s)	31 atm
II	4.5 CH_4 - 2 O_2 - 2 He	448 (m/s)	31 atm
III	3.5 CH_4 - 2 O_2 - 6.5 He	544 (m/s)	31 atm
IV	0.6 C_2H_4 - 2 O_2 - 3.3 CO_2	291 (m/s)	16 atm

Fig. 11 Velocity profile in thermally choked and superdetonative ram accelerator modes.

V. THEORETICAL MODELING

In the superdetonative ram accelerator operation mode (Fig.2) ignition of the fuel/oxidizer mixture is achieved by means of a series of shock waves that increase its temperature until the ignition temperature is reached at some desired location. At this point, rapid chemical reactions release energy into the flowing stream. The energy addition will establish either a detonation wave or a coupled or decoupled shock-deflagration system, depending primarily on the mixture composition, pressure and tube size. The combustion process creates a high pressure region over the back of the projectile, producing a thrust force. The pressure, composition, chemical energy density and speed of sound of the mixture can be controlled to optimize the performance for a given flight condition.

Computational fluid dynamics (CFD) is playing a major role in the development of hypersonic propulsion[18,19], due to its ability to predict, in principle, all the relevant flow and combustion phenomena at conditions for which experimental facilities do not currently exist. At the University of Washington, a CFD capability has also been under development, in support of the experimental effort, almost since its conception.[9,10,20,21] These studies have improved our understanding of the ram accelerator, and will certainly continue to provide new information necessary for the achievement of higher speeds.

The CFD code discussed here has been used to analyze the performance of various ram accelerator configurations in the superdetonative velocity range of 4.0 to 9.0 km/s. Due to the similarity between the flow and combustion processes in the ram accelerator and those associated with hypersonic airbreathing engines, it is clear that the numerical studies presented here also have direct value to the latter.

Numerical Formulation

The complete numerical scheme used for the present study is described in detail in Appendix A and in Refs. 9 and 21, and therefore will only be discussed in general terms here. The governing equations, the Euler equations coupled with chemical nonequilibrium processes, are solved using a shock-capturing technique applied to flows around a ram accelerator configuration. The equations are written in nondimensional variables and in general curvilinear coordinates. Real gas effects are taken into account by expressing the specific heats of the various species as a function of temperature. The corresponding expressions were obtained from the JANAF tables.[22]

A combustion model for hydrogen/oxygen mixtures consisting of 8 reactions and 7 species, including 6 reacting species H, O, H_2O, OH, O_2, H_2, and an inert specie, such as Argon or Nitrogen, was selected for our computations.[23] The eight reactions assumed to be significant are:

$$H + O_2 \Leftrightarrow OH + O$$

$$O + H_2 \Leftrightarrow OH + H$$

$$H_2 + OH \Leftrightarrow H + H_2O$$

$$2OH \Leftrightarrow H_2O$$

$$H_2 + X \Leftrightarrow 2H + X$$

$$H_2O + X \Leftrightarrow OH + H + X$$

$$OH + X \Leftrightarrow O + H + X$$

$$O_2 + X \Leftrightarrow 2O + X$$

The forward and backward reaction rates, K_{fi} and K_{bi}, are given by expressions of the form

$$K_i = A_i T_{bi} e^{-Ci/T} \qquad (1)$$

The reaction coefficients A_i, b_i and C_i were taken from Evans and Schexnayder.[24]

The 2D/axisymmetric code employs the "Point Implicit TVD MacCormack" time marching method to solve the complete Euler and species equations in a fully coupled manner.[25,26] This approach requires an implicit treatment of the chemical source term, due to the fact that the equation set is mathematically stiff. The degree of stiffness is determined by the Damköhler number, defined as the ratio of the characteristic convection time to the characteristic reaction time. High Damköhler numbers imply high levels of stiffness, and in general there will be a Damköhler number associated with each reaction in the chemistry model.

Besides solving the stiffness problem, this method has several desirable properties, such as high-order accuracy, robustness, and the ability to achieve high resolution of shock waves, without the spurious oscillations associated with the more classical high-order

schemes. The main disadvantage of the method is, however, that the solutions are not, in general, time accurate, making the scheme suitable only for steady state calculations.

The boundary conditions are specified as follows: The flow is supersonic ahead of the projectile so that all flow variables are known. The flow remains supersonic throughout the ram accelerator and, therefore, we can impose a zero-gradient outflow condition. The wall boundaries are specified by the following procedure: The velocity components u and v at the wall are obtained from the condition of zero normal velocity component at the wall. The pressure is obtained by solving the normal momentum equation at the wall. In the results presented here, the wall was assumed to be adiabatic and fully non-catalytic, which implies that the total enthalpy, h_0, is constant, and that the normal gradient of each species mass fraction, c_i, is zero at the wall:

$$\left(\frac{\partial c_i}{\partial n}\right)_{wall} = 0 \tag{2}$$

The gas temperature, T, at the wall is then obtained from the definition of total enthalpy

$$h_o = \sum_{i=1}^{n} c_i \int^{T} c_{p_i}\, dT + \frac{1}{2}(u^2 + v^2) + \sum_{i=1}^{n} c_i\, h_i^o \tag{3}$$

where c_{p_i} is the specific heat at constant pressure of the ith species, and h_i^o is the heat of formation for species i. An iterative method is used to solve for T. The density, ρ, at the wall is obtained from the equation of state

$$\rho = \frac{p}{\sum_n^{i=1} \frac{c_i}{M_i} R T} \tag{4}$$

where M_i is the molecular weight of the ith species, and R is the universal gas constant. Finally, the species densities, ρ_i, are obtained from the relation ri=cir. (A complete discussion of the boundary conditions is given in Ref. 21).

Results

The numerical scheme described above, has been validated/calibrated by using benchmark test cases for which analytical, numerical or experimental results are available.[9,21] Two such validation test cases are presented here, preceding the discussion of the numerical studies conducted on the ram accelerator.

Benchmark Test Cases

Figures 12 to 15 present two of several test cases conducted on the "exothermic blunt body flow" problem. This type of flow, which consists of blunt projectiles flying into detonable gas mixtures, covers a wide range of shock-induced phenomena; from decoupled and coupled shock-deflagration systems, to overdriven and oblique detonation waves. They were experimentally investigated in the mid 1960's[27,28] and early 1970's, most notably by a group of researchers at the Institute Franco-Allemand de Recherches de Saint-Louis.[29,30]

Figures 12 and 13 show a comparison between experimental and computational results obtained by using the present numerical scheme, for a spherical projectile flying through a stoichiometric mixture of H_2 / O_2 at a pressure of 186 torr, and a Mach number M=3.55 (subdetonative speed). The experimental results were obtained from the work of Lehr.[30] This case, produced a decoupled shock-deflagration system, in which the combustion front is separated from the shock wave by an induction zone. The numerical calculation shown in Fig. 13, which consists of nondimensional temperature contours, successfully reproduced the decoupled shock-deflagration system. The shock wave, induction zone and combustion front can be clearly identified. The experimentally observed shock location, taken from Fig. 12, is also shown for comparison.

Figures 14 and 15 show the same comparison for a Mach number M=5.08 (superdetonative speed). A combination of overdriven and oblique Chapman-Jouguet detonation waves is obtained in this case. Although the detailed structure of the detonation is not resolved numerically, the overall effects such as the location of the overdriven portion of the wave, and the angle and location of the oblique portion, are in close agreement with experiment.

The benchmark computations presented here as well as those reported in Refs. 9 and 21, have provided the means for assessing the accuracy of the numerical scheme. Extension to ram accelerator configurations can then be carried out, and they are presented below.

Fig. 12 Shock wave and combustion front in a stoichiometric H_2/O_2 mixture at M = 3.55 (from Ref. 30).

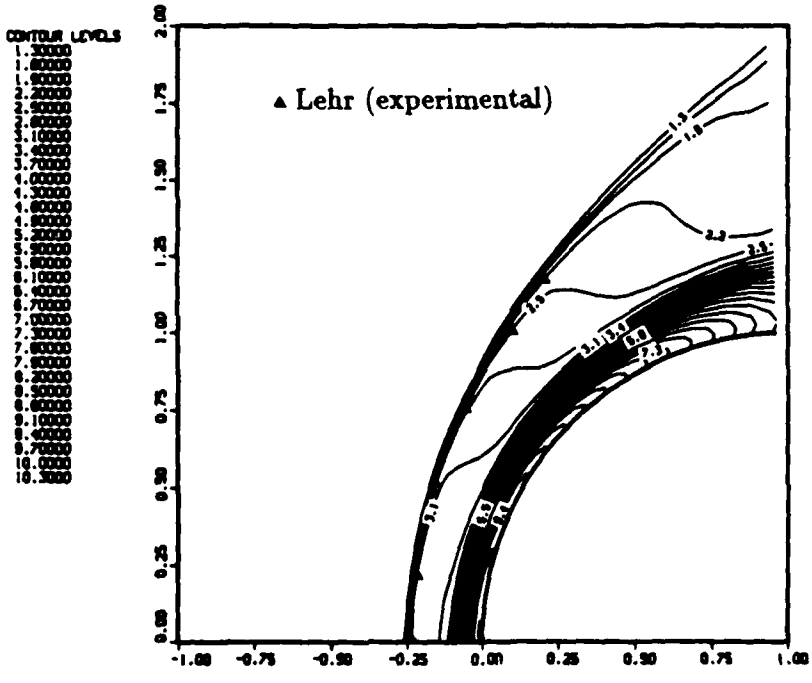

Fig. 13 Temperature contours (T/T_∞) for stoichiometric H_2/O_2, M = 3.55 flow past a sphere. Experimental shock location obtained from Fig. 12.

Fig. 14 Overdriven detonation and oblique Chapman-Jouguet detonation in a stoichiometric H_2/O_2 mixture at M = 5.08 (from Ref. 30).

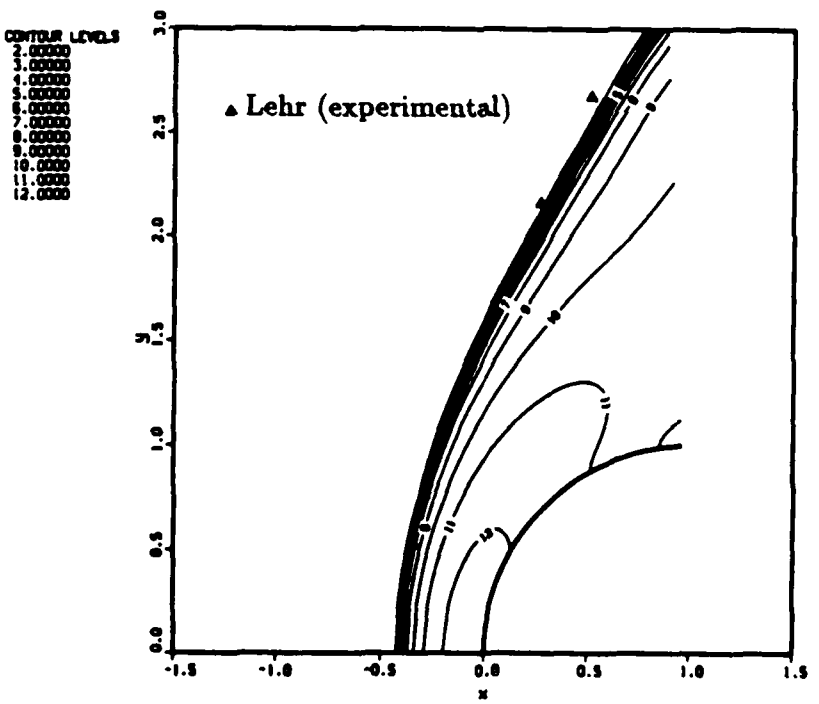

Fig. 15 Temperature contours (T/T_∞) for stoichiometric H_2/O_2, M = 5.08 flow past a sphere. Experimental shock location obtained from Fig. 14.

Ram Accelerator Configuration

The results to be presented on the ram accelerator do not represent a complete parametric study of this concept. The main purpose of these studies is to indicate general performance trends, and to analyze the effects that the different parameters, such as Mach number, projectile shape, projectile-to-wall area ratio, and gas mixture, have on the flow, combustion, and performance characteristics of the ram accelerator.

Most of the calculations associated with the ram accelerator configuration were carried out on a 155 x 21 patched grid. A typical grid is shown in Fig. 16, where the plot has been magnified by a factor of 5 in the vertical direction for clarity. The same projectile configuration on a 1:1 scale is shown in Fig. 17.

Performance as a Function of Mach Number

Optimum performance is obtained by keeping the projectile Mach number within a narrow range. This can be accomplished by dividing the launch tube into several segments filled with different propellant mixtures, and constraining the projectile to operate over a limited Mach number range in each segment.

Figures 18 to 21 show the effects of Mach number on the flow and combustion phenomena in a ram accelerator tube section filled with a gas mixture of $2H_2 + O_2 + 5He$ at a typical fill pressure of 20 atm. A projectile configuration (Fig. 17) having dimensions close to those of the experimental device presently operating at the University of Washington was chosen for this study. The projectile is composed of two 14° half angle cones and a cylindrical section. The maximum projectile radius is 1.45 cm and its length is 19 cm. The tube radius is 1.9 cm.

Figure 18 shows temperature contours and the temperature distribution along the projectile surface and tube wall for a Mach number M = 7 (flight speed U_1 = 5.2 km/s). The contour plot is magnified in the vertical direction by a factor of 5. The numerical solution shows the crisp shock waves captured by the method. At these flight conditions, the shock wave system generated by the projectile is not strong enough to ignite the mixture. Therefore, no combustion and no thrust are generated in this case.

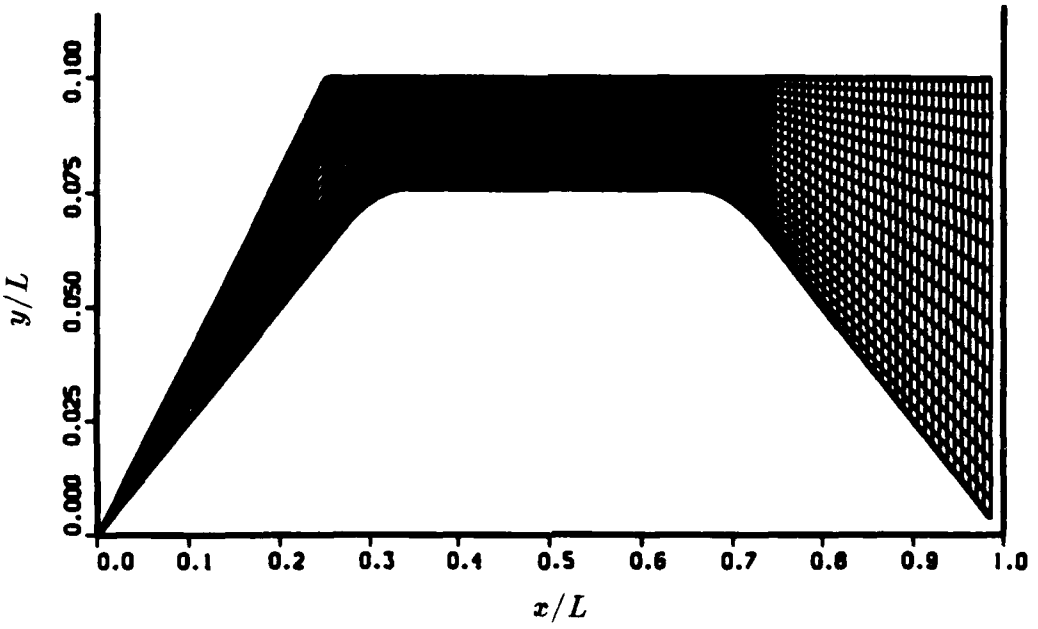

Fig. 16 Typical grid for the ram accelerator. Vertical axis is magnified by a factor of 5.

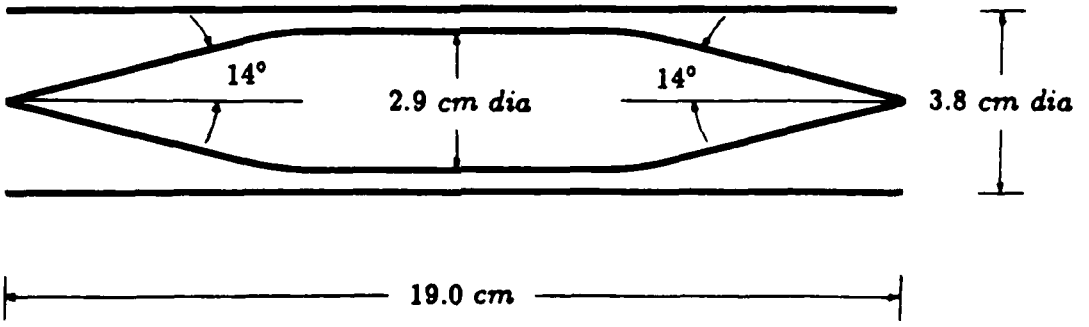

Fig. 17 Ram accelerator projectile configuration on a 1:1 scale.

a)

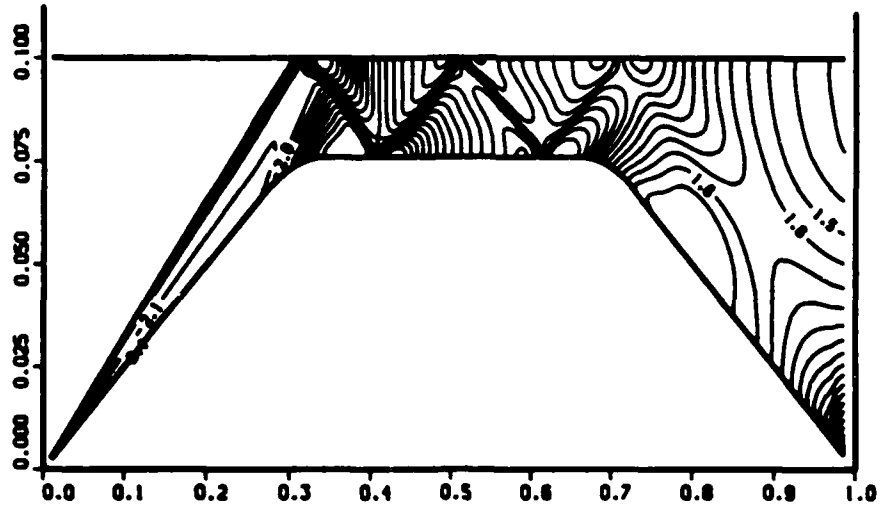

b)

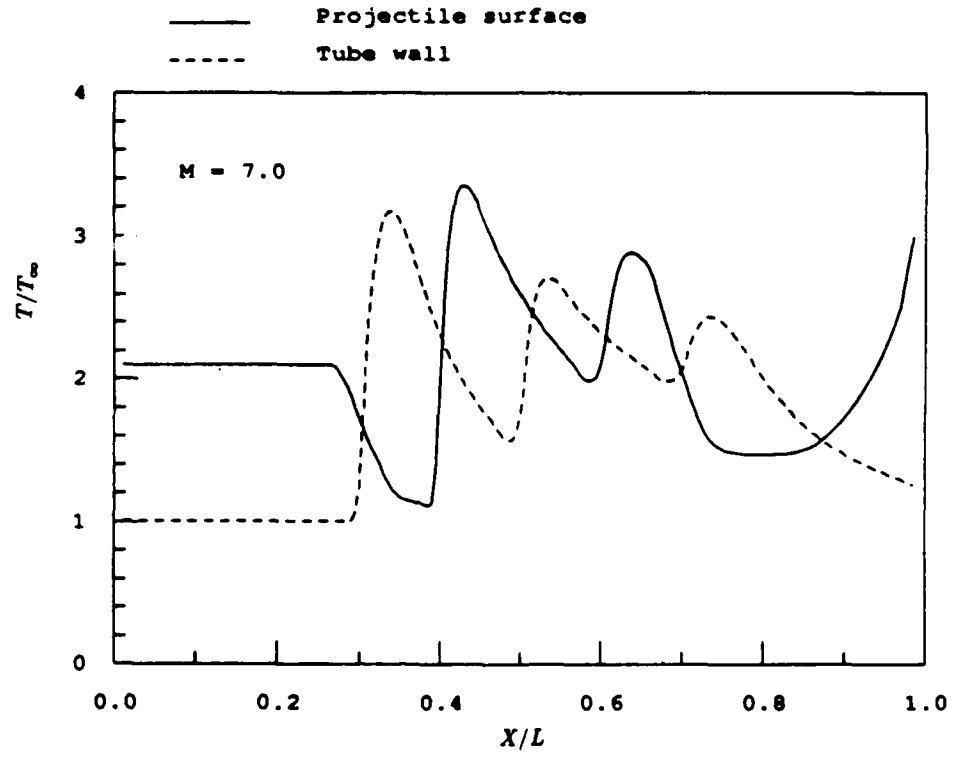

Fig. 18 (a) Temperature contours T/T_∞; (b) Temperature distribution; for a 14∞ projectile. U_1 = 5.2 km/sec (M = 7), mixture: $2H_2 + O_2 + 5He$.

a)

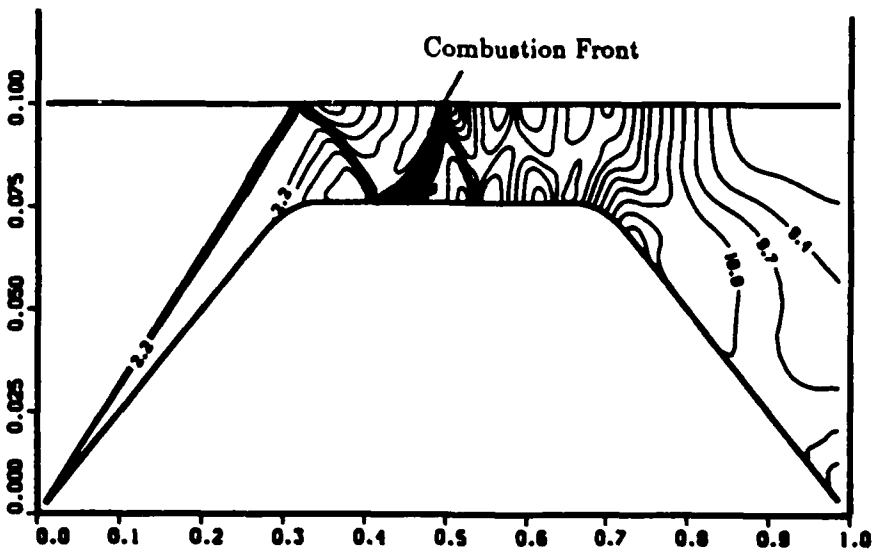

b)

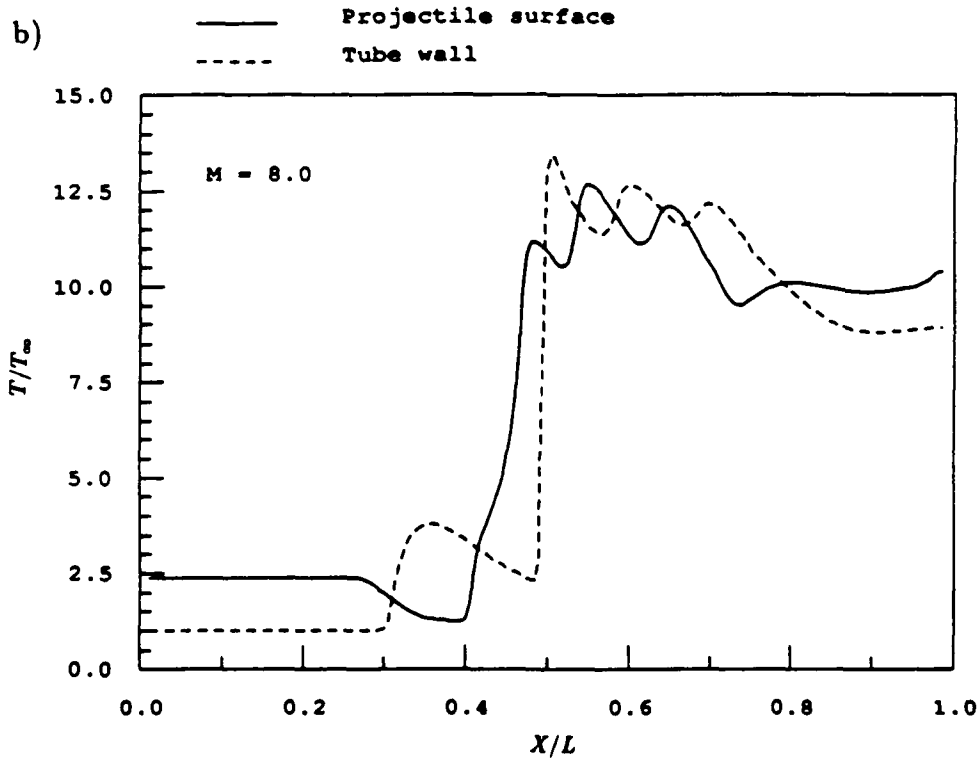

Fig. 19 (a) Temperature contours T/T_∞; (b) Temperature distribution; for a 14∞ projectile. $U_1 = 5.9$ km/sec (M = 8), mixture: $2H_2 + O_2 + 5He$.

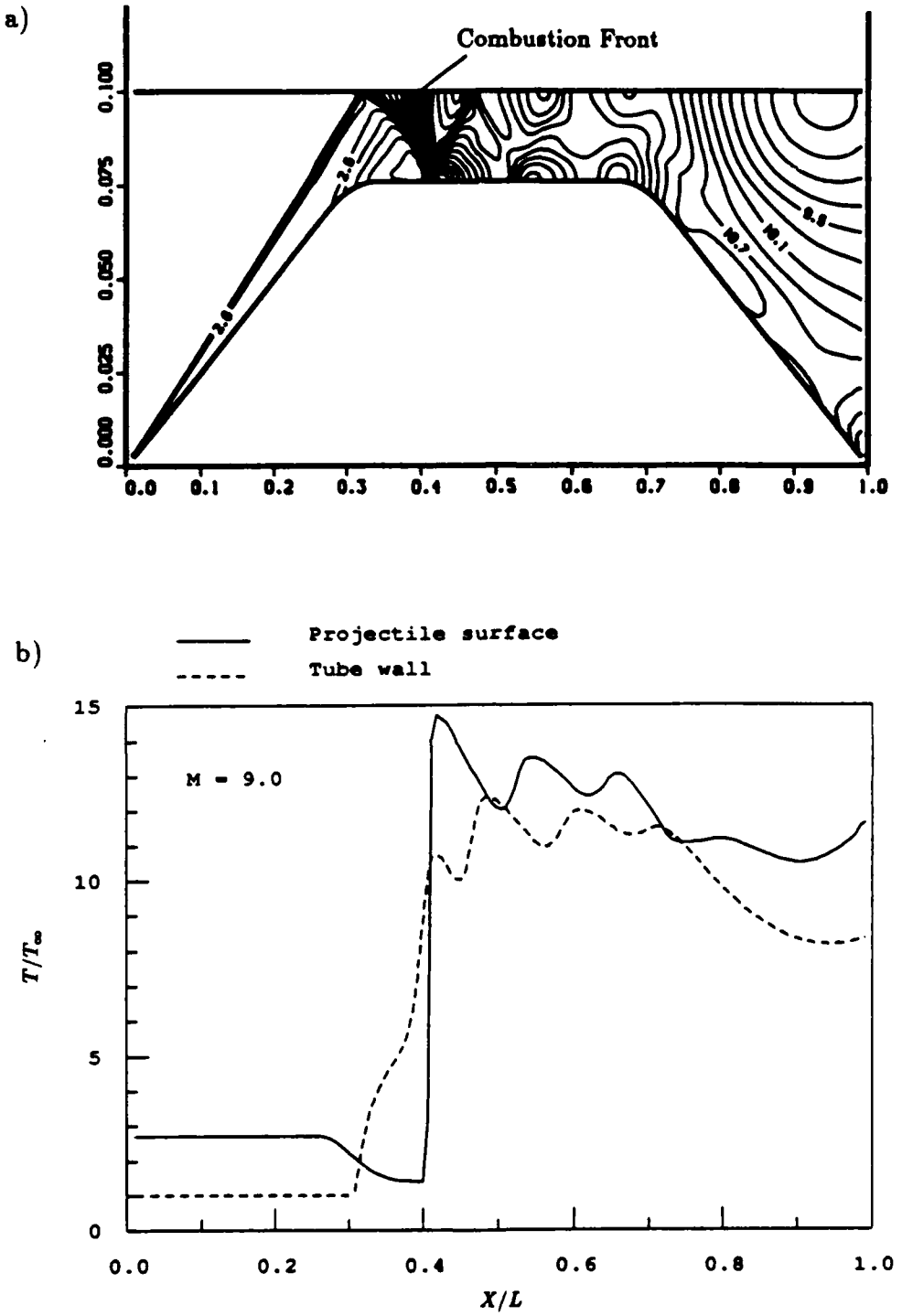

Fig. 20 (a) Temperature contours T/T_∞; (b) Temperature distribution; for a 14∞ projectile. U_1 = 6.7 km/sec (M = 9), mixture: $2H_2 + O_2 + 5He$.

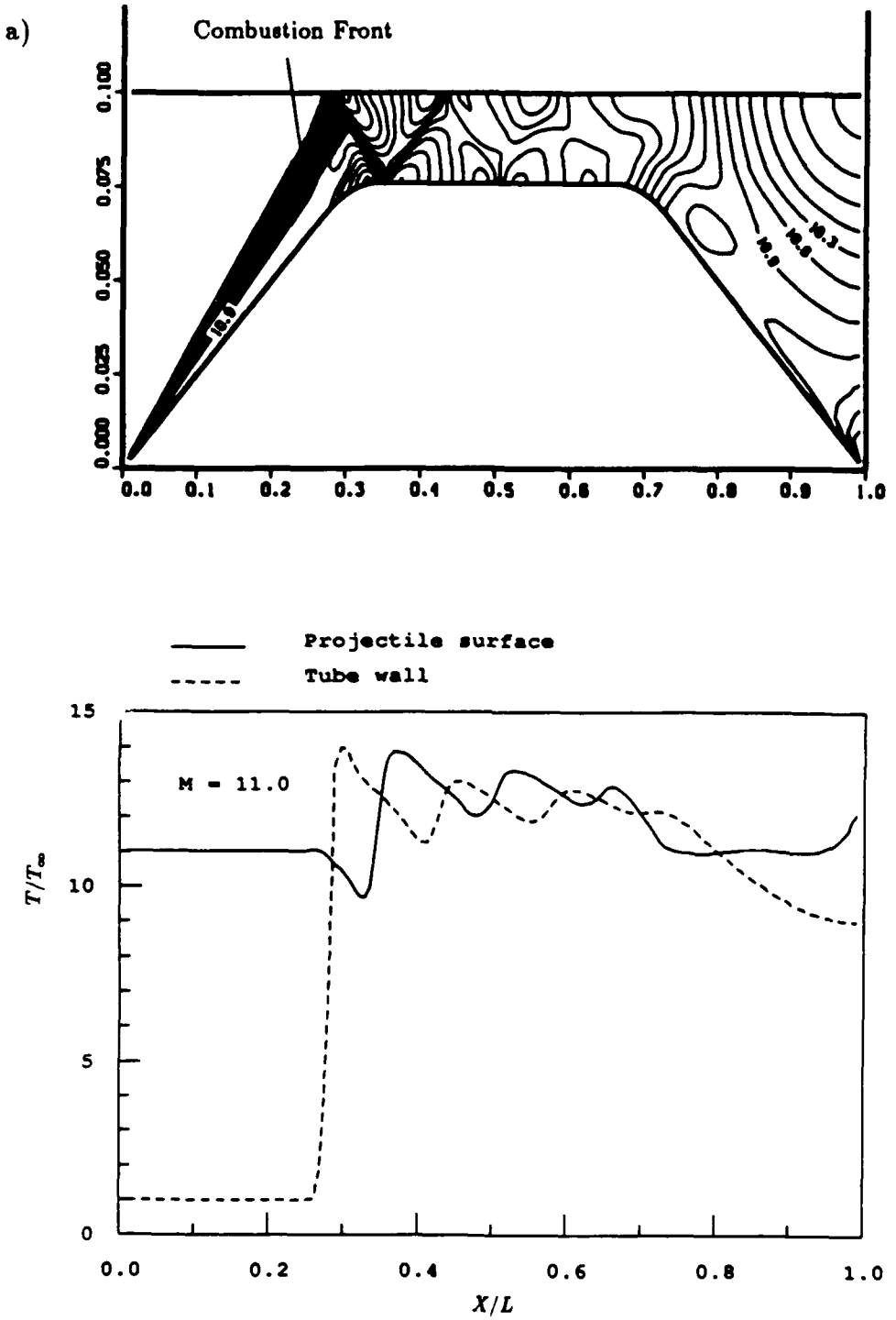

Fig. 21 (a) Temperature contours T/T_∞; (b) Temperature distribution; for a 14∞ projectile. U_1 = 8.1 km/sec (M = 11), mixture: $2H_2$ + O_2 + 5He.

A higher flight speed is required in order to ignite the mixture. Figure 19 shows the results for a Mach number M = 8 (U_1 = 5.9 km/s). At this Mach number, ignition is reached behind the second shock reflection, and rapid chemical reactions release energy into the flowing stream establishing a shock-induced combustion front. Shown in the contour plot are the nose bow shock and its reflection from the tube wall, followed by the combustion front and the expansion wave system over the tail of the projectile. A positive thrust force is produced at this flight condition.

The combustion front will remain behind the second shock reflection for a certain Mach number range. As the projectile accelerates inside the tube, the strength of the shock wave system increases and, at a given point, causes the combustion front to jump from the second shock reflection to the first. This situation is shown in Fig. 20 for a Mach number M = 9 (U_1 = 6.7 km/s). Note that due to the effect of the second reflection, which tends to speed up the reactions, the combustion zone at the projectile surface is narrower than at the tube wall.

The upper end of the operating velocity range is reached when the strength of the nose bow shock is sufficiently high to initiate combustion prematurely. For the present projectile configuration and gas mixture, this upper limit is reached near M = 11 (U_1 = 8.1 km/s). This case is shown in Fig. 21. It is important to point out that for all the above cases, the flow remains supersonic throughout the length of the projectile.[9,21]

The pressure distribution along the projectile surface and tube wall for the four cases discussed above is shown in Figs. 22 to 25. Note that for the M = 8 and M = 9 cases the pressure at the projectile tail is higher than that at the nose, and as a result, a positive thrust force is produced.

A nondimensional thrust, $\tilde{F}$, can be defined as:

$$\tilde{F} = \frac{F}{p_\infty A_t} \tag{5}$$

where F is the thrust, p_1 is the fill pressure, and A_t is the tube area. For the M = 8 and M = 9 cases thrust forces $\tilde{F}$ = 3.27 and $\tilde{F}$ = 2.93 were obtained respectively. For the M = 7 case, where no combustion occurred, $\tilde{F}$ =-2.16, which represents, in fact, the projectile wave drag.

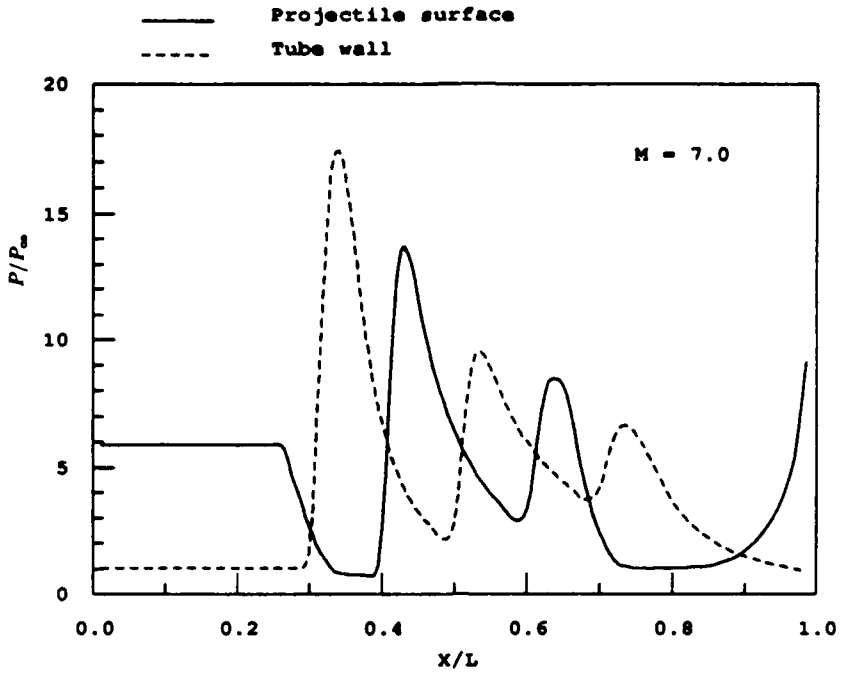

Fig. 22 Pressure distribution along the tube wall and projectile surface for the M = 7 case.

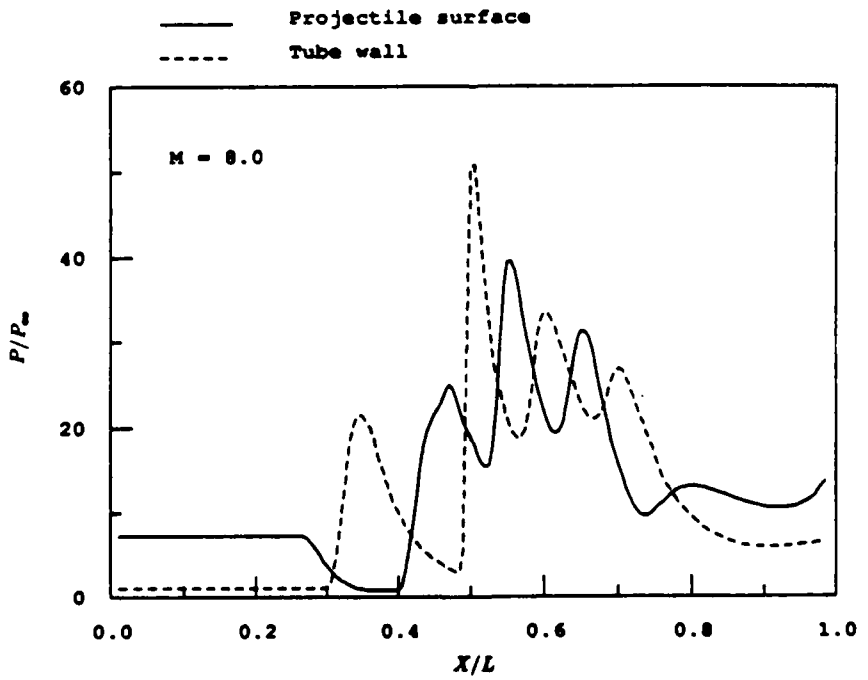

Fig. 23 Pressure distribution along the tube wall and projectile surface for the M = 8 case.

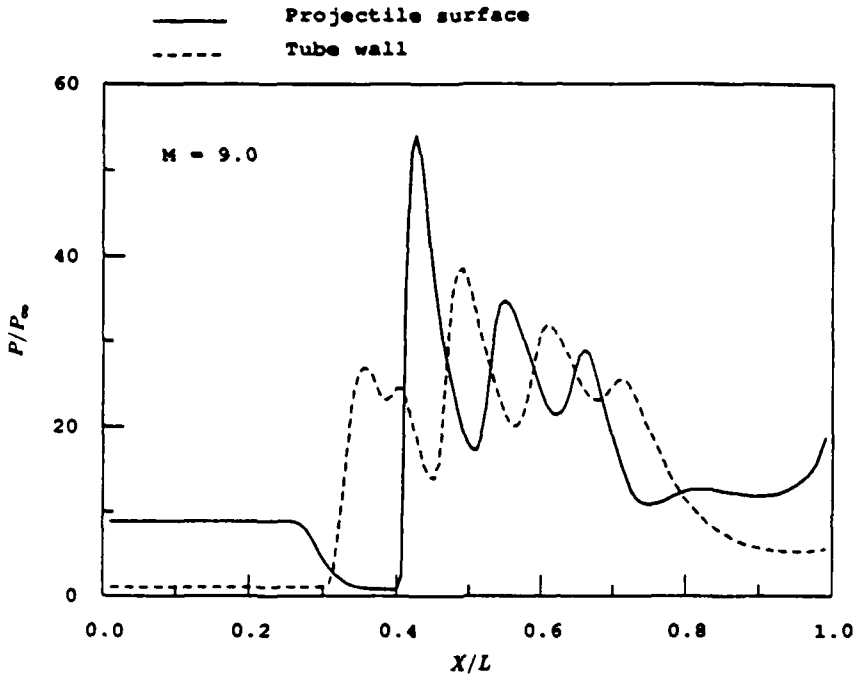

Fig. 24 Pressure distribution along the tube wall and projectile surface for the M = 9 case.

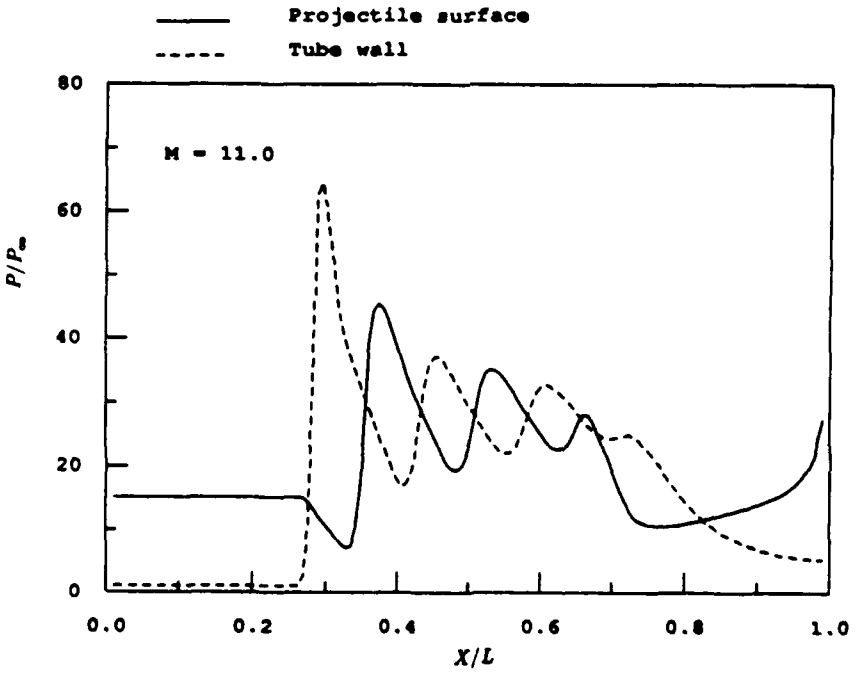

Fig. 25 Pressure distribution along the tube wall and projectile surface for the M = 11 case.

The M = 11 case is particularly interesting, since, although it resulted in a net drag force, $\tilde{F} = -0.61$, its value was almost an order of magnitude lower than that obtained for the same flight conditions but with the assumption that the flow is frozen (no chemical reactions), in which case $\tilde{F} = -5.1$. This indicates that part of the chemical energy released can still be utilized for thrust production. A similar result was observed experimentally by Ruegg and Dorsey[27], who noted a large reduction of the drag coefficient of spherical missiles fired into detonable mixtures, when combustion was established in the shocked gas. They even suggested the possibility of attaining positive thrust by properly shaping the projectile, however, to the best of our knowledge this was never attempted.

Ballistic Efficiency and Thrust Pressure Ratio

The performance of the ram accelerator can be characterized by two main parameters: ballistic efficiency and thrust pressure ratio. The ballistic efficiency, η_b, is defined here as the ratio of the rate of change of kinetic energy of the projectile to the rate of expenditure of chemical energy. It can be expressed in the following way

$$\eta_b = \frac{FU_1}{\dot{m}\Delta q} \tag{6}$$

where U_1 is the projectile speed, $\dot{m}$ is the mass flow rate and Δq is the heat per unit mass released into the flow. The thrust pressure ratio, Φ_t, is the net average drive pressure on the projectile (the thrust divided by the maximum projectile cross-sectional area) divided by the maximum cycle pressure. This ratio is an important performance parameter because it provides a measure of the device's launch capability versus the maximum pressure the projectile and launch tube must survive.

Figure 26 shows the variation of ballistic efficiency as a function of projectile speed for two different projectiles, one having nose and tail half angles of 12° and the other 14°. The lowest speed data point in each case corresponds to a combustion front behind the second shock reflection, while the highest speed corresponds to premature combustion at the bow shock. Note that the 12° projectile produces a very small positive thrust in the case of

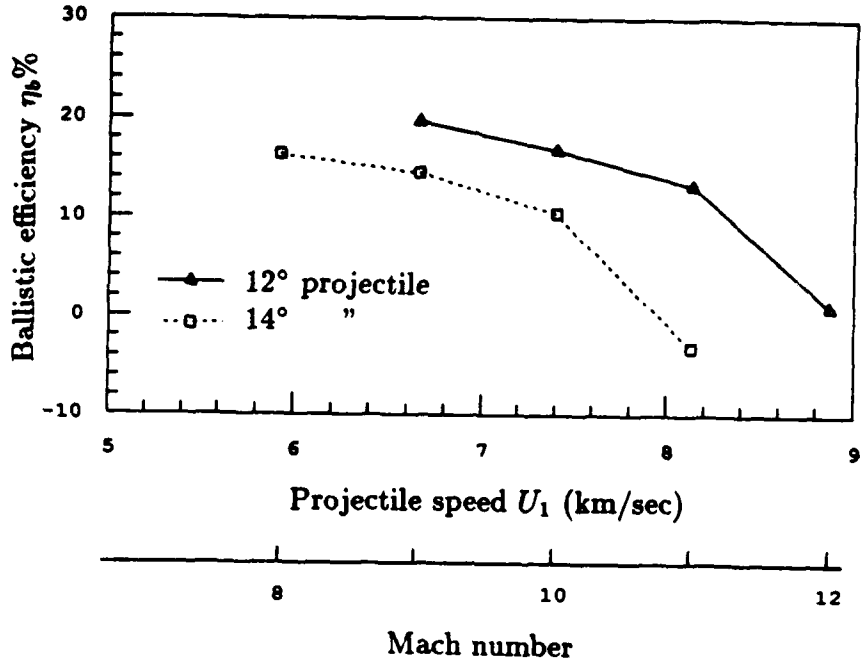

Fig. 26 Ballistic efficiency as a function of ram accelerator projectile speed and Mach number for two projectile geometries. Mixture: $2H_2 + O_2 + 5He$.

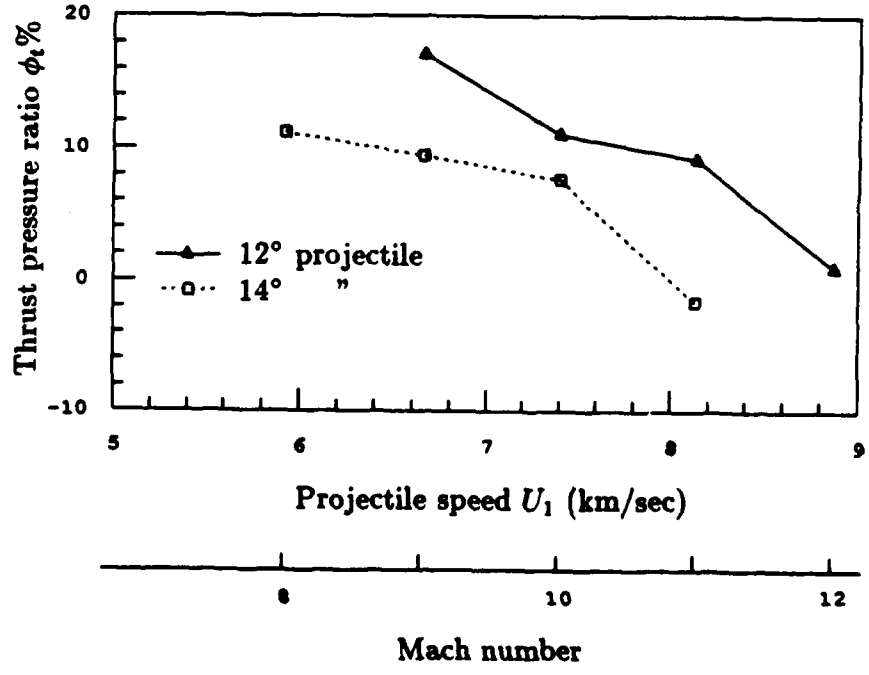

Fig. 27 Thrust pressure ratio as a function of ram accelerator projectile speed and Mach number for two projectile geometries. Mixture: $2H_2 + O_2 + 5He$.

premature combustion. It is observed that higher efficiencies are obtained with the 12° nose projectile (up to 20%), however, it must operate at higher speeds and Mach numbers. The operational Mach number range of the 12° projectile is approximately from M = 9 to M = 11, while that of the 14° is from M = 8 to M = 10. For a given projectile, the ballistic efficiency decreases with increasing speed. This is due to the fact that the high pressure region behind the combustion zone is not very sensitive to changes in speed, while the nose wave drag increases significantly as the projectile speed increases.

Thrust pressure ratio results are shown in Fig. 27. Here, Φ_t is plotted versus projectile speed. The trends shown here are similar to the trends shown for η_b in Fig. 26. Values of Φ_t as high as 17% are obtained.

Performance as a Function of Area Ratio

Figure 28 shows the ballistic efficiency of two projectiles (having 12° and 14° nose/tail half angles) as a function of projectile-to-tube area ratio, A_p/A_t, where A_p and A_t are the cross-sectional areas of the projectile and tube, respectively. The effect of increasing A_p/A_t is to increase the ballistic efficiency. The ballistic efficiency is increased by approximately 50% in going from $A_p/A_t = 0.52$ to $A_p/A_t = 0.70$. There is however, a practical limitation on the maximum value of the area ratio. At values of A_p/A_t approaching 1, the boundary layer on the projectile will extend up to the tube wall, reducing the efficiency of the system.

The thrust pressure ratio variation with A_p/A_t is shown in Fig. 29. Changing the area ratio does not appear to have a specific effect on Φ_t, and it remains nearly constant. The small variations are probably associated with the wave interactions taking place for a particular geometric configuration.

Blunt Nose Effects

A numerical investigation of the effects of nose blunting on the flow and combustion processes in the ram accelerator was performed. The purpose of this study was was to determine under what conditions a high temperature, thin entropy layer, originating from the nose stagnation region might be established, and what the interaction between this entropy layer and the reflected shock-wave coming from the tube wall would be. This study is important, since there is a possibility that such an entropy layer, consisting of high temperature combustion products, may be generated even with slight blunting of the nose, and may actually be the ignition source for the combustion processes in the ram accelerator.

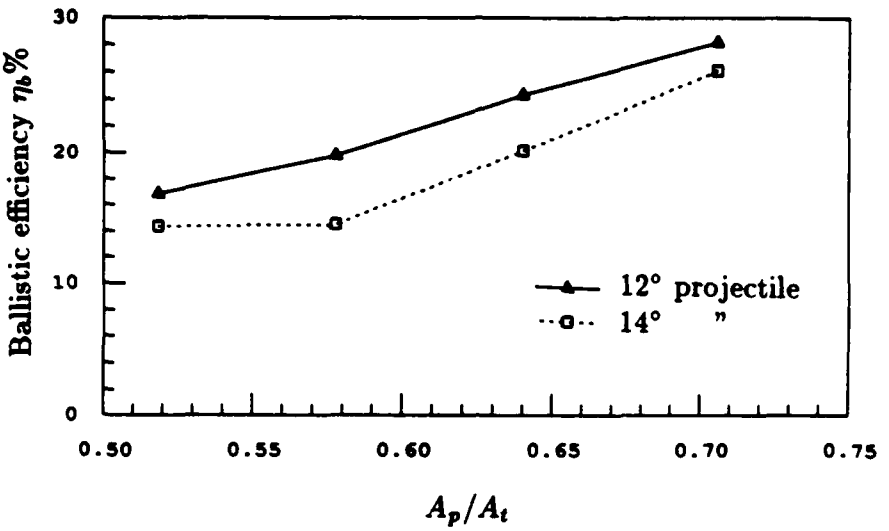

Fig.28 Ballistic efficiency as a function of projectile-to-tube area ratio. Mixture: $2H_2 + O_2 + 5He$.

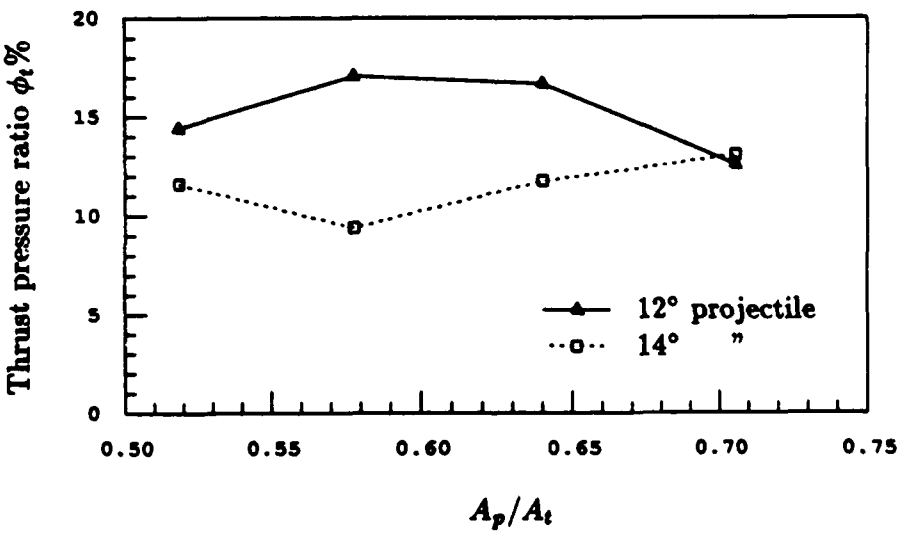

Fig.29 Thrust pressure ratio as a function of projectile-to-tube area ratio. Mixture: $2H_2 + O_2 + 5He$.

The results of such a calculation are shown in Figs. 30 to 35. The projectile is composed of a 10° half angle cone with a spherical nose of radius 0.6 mm, and a cylindrical section of radius 1.6 mm. A stoichiometric H_2/air mixture at a pressure of 10 atm was considered. The Mach number is M = 4.2 in the present case.

Figure 30 shows temperature contours. A high temperature, thin entropy layer consisting of combustion products is established under these conditions, extending along the entire projectile surface. The nose region is shown in more detail in Fig. 31. The nose bow shock wave is reflected from the tube wall and it then interacts with the entropy layer. Note that in this interaction, the entropy layer remains attached to the body. However, the way in which the shock wave is reflected from the projectile surface is affected by the presence of the entropy layer. Figure 32, which consists of nondimensional pressure contours, shows that the shock reflection at the surface is actually a Mach reflection. In this type of reflection, a nearly normal shock that appears near the projectile surface forms a triple intersection point with the incident and "reflected" shock. This effect is more clearly seen in Fig. 33, which shows the particle traces. Behind the nearly normal shock, the streamlines are nearly parallel to the projectile surface and the flow is subsonic there. Also, since the streamlines behind the "reflected" shock are not parallel to the projectile surface, the triple point must be actually a short region in which the nearly normal shock continuously curves into the "reflected" shock rather than being a true discontinuity. In the case of nonreacting flow, a "regular" reflection was observed. However, inside the entropy layer of the reacting flow case, the gas properties are such that a "regular" reflection is impossible.

The effects of viscosity in this type of interaction should be investigated, since it may provide a physical mechanism to diffuse the high temperature entropy layer into the main flow. A full Navier-Stokes simulation would be required in this case.

A second effect we wanted to investigate was the effect of combustion on the pressure distribution on the projectile surface. Figure 34 shows a comparison between the results obtained for the chemically reacting case and those that would be obtained if no chemical reactions were allowed (frozen flow), keeping all the other parameters equal. The horizontal coordinate, S/R, in Fig. 34 represents the nondimensional distance along the projectile surface. Note that the combustion process has almost no effect on the pressure distribution. This effect is generally observed in unconfined chemically reacting flows. For example, Prabhu[31] found very small effects on the surface pressure distribution for flows past spheres, in the case of endothermic chemical reactions related to equilibrium air. This effect is very important to the

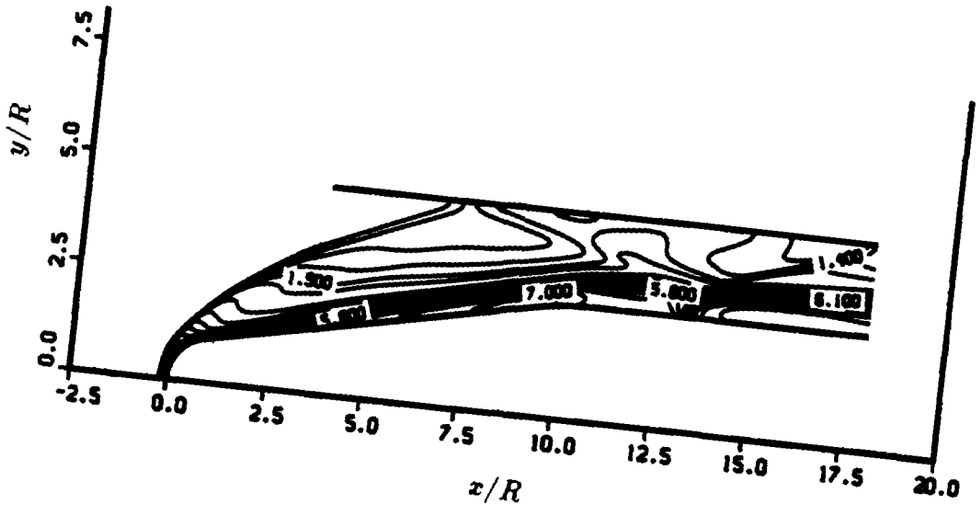

Fig. 30 Temperature contours (T/T_∞) for a blunt projectile. M = 4.2, nose radius R = 0.06 cm, mixture: stoichiometric H_2/air.

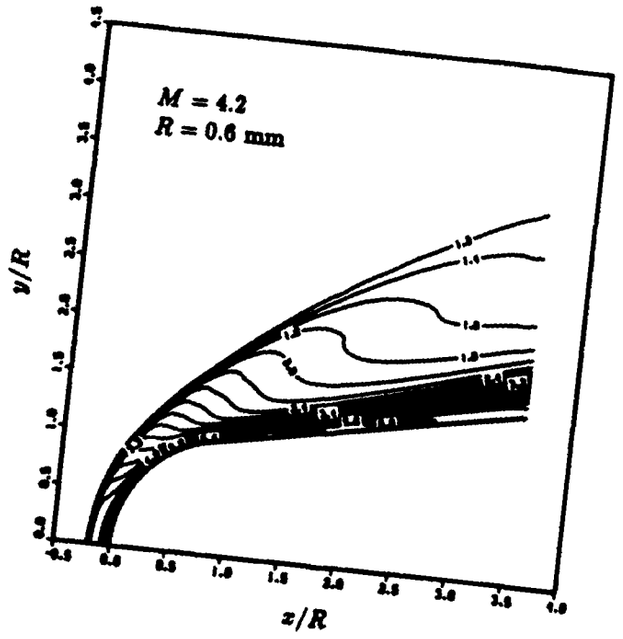

Fig. 31 Temperature contours (T/T_∞) in the nose region of the blunt projectile.

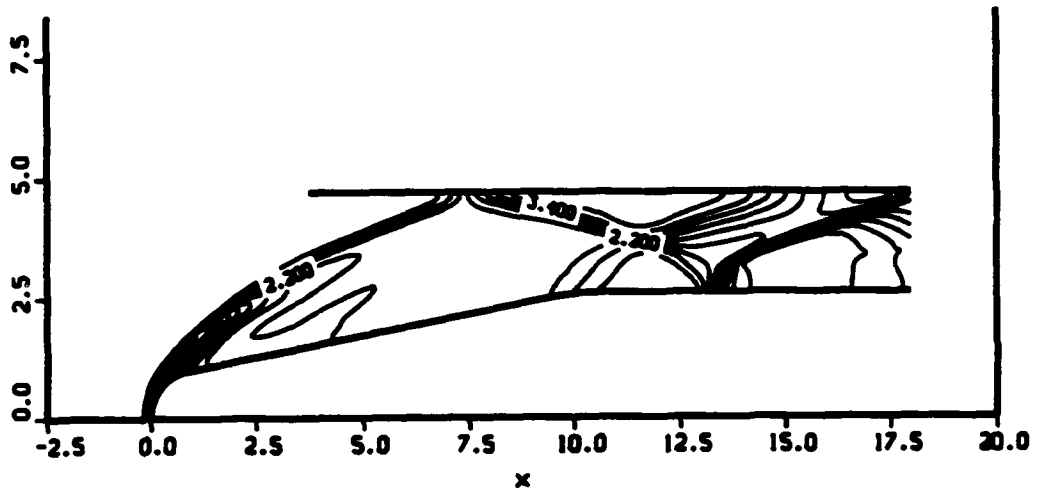

Fig. 32 Pressure contours (p/p_∞) for a blunt projectile. M = 4.2, nose radius R = 0.06 cm, mixture: stoichiometric H_2/air.

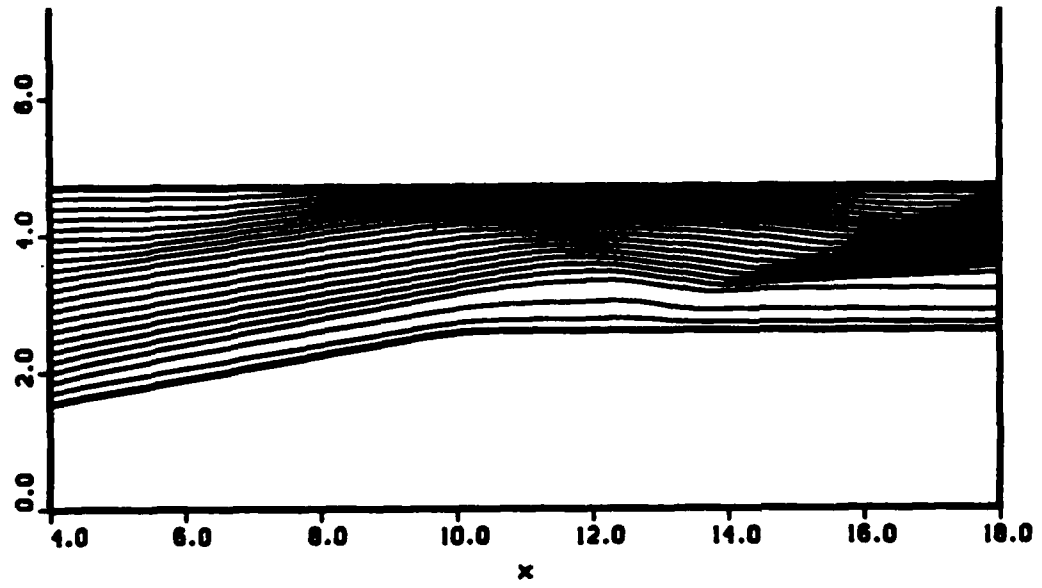

Fig. 33 Particle traces for the blunt projectile.

ram accelerator concept, since it indicates that some combustion occurring in the nose area of the projectile can be allowed, and this will not cause an increase in pressure over the frontal part of the projectile and, therefore, it will not cause a significant reduction in thrust.

As a final comment, Fig. 35 shows the temperature distribution along the projectile surface for the reacting and frozen flow cases. It is interesting to note that in the reacting case, the maximum temperature does not occur at the stagnation point but rather at a location on the spherical nose of the body corresponding to an angular distance of approximately 50° from the stagnation point. This is caused by the fact that the flow is in chemical nonequilibrium. If we consider a flow particle moving along the stagnation streamline, the above results indicate that it will not reach complete combustion at the stagnation point, but rather it will continue to react along the body surface. Complete combustion is attained near the 50° location, after which, due to the expansion process in this area of the body, the temperature begins to decrease.

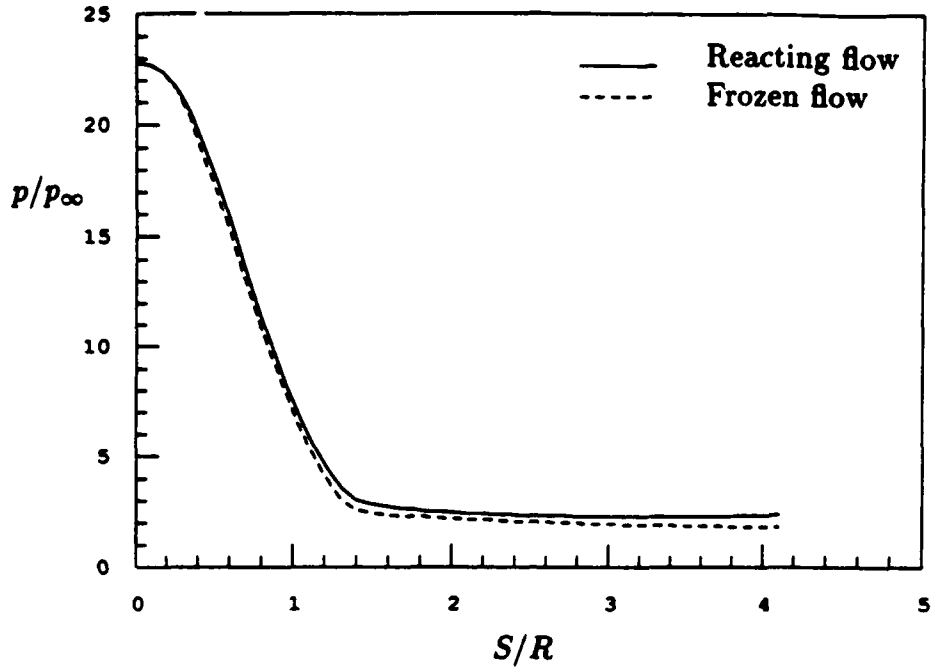

Fig. 34 Comparison of pressure distribution on the projectile surface for reacting and frozen flows.

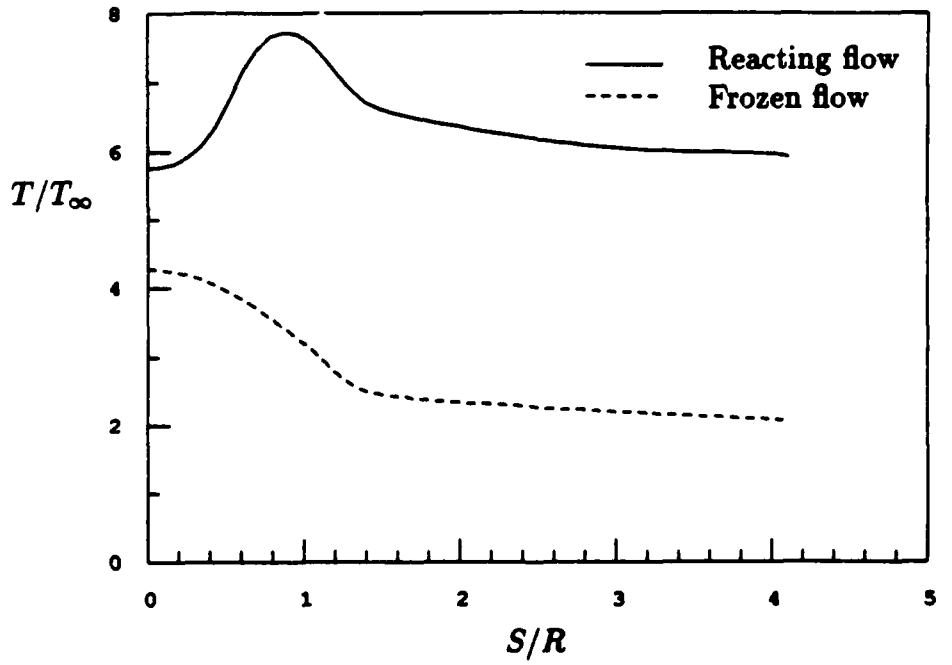

Fig. 35 Comparison of temperature distribution on the projectile surface for reacting and frozen flows.

VI. CONCLUSIONS

Acceleration of projectiles by ram accelerator propulsive modes at velocities greater than the local C-J detonation speed has been experimentally demonstrated in both methane and ethylene-based propellant mixtures and has been theoretically investigated in hydrogen mixtures. Projectiles were accelerated through the velocity range of 2000 m/sec to near 2500 m/sec by an ethylene-oxygen-carbon dioxide propellant mixture having an experimentally determined detonation speed of 1650 m/sec. Theoretical investigations indicate that superdetonative operation may efficiently accelerate projectiles to near 9 km/s. Many propellant mixtures used in the thermally choked propulsive mode have demonstrated extraordinary accelerations when the projectiles have been allowed to approach the detonation velocity of the mixture, and in several methane based propellant mixtures the projectiles have been smoothly accelerated through the entire transdetonative regime (85%-115% C-J detonation speed). These experiments suggest that smooth acceleration from a low Mach number, subdetonative regime to a hypersonic, superdetonative regime may be possible in a single propellant mixture.

An inviscid TVD numerical scheme, which includes nonequilibrium chemistry, real gas effects and a 7 species-8 reaction combustion model was used to investigate the flow, combustion, and performance characteristics of various ram accelerator configurations in the superdetonative velocity range. The ballistic efficiency and thrust pressure ratio increased when the projectile nose and tail angles were reduced, however, the ram accelerator would have to operate at higher Mach numbers. The ballistic efficiency increased with increasing projectile-to-tube area ratio. This area ratio had no significant effect on the thrust pressure ratio. Ballistic efficiencies of up to 28% and thrust pressure ratios as high as 17% were observed. The effects of nose blunting on the flow and combustion processes in the ram accelerator were also investigated. Under the assumption of inviscid flow, it was found that the high temperature, thin entropy layer produced under certain conditions, remains attached to the body even in the region behind the reflected shock wave impinging upon it. However, the presence of the entropy layer created a Mach reflection at the projectile surface. Viscous effects on this shock-entropy layer interaction should be investigated. This limited combustion layer had a very small effect on the pressure distribution at the projectile surface. Therefore, we can conclude that limited combustion can be allowed to take place in the frontal area of the projectile, without severely reducing the thrust force in the ram accelerator. Even in the most severe case of full premature combustion at the bow shock, a drag reduction (and sometimes even a very small positive thrust force) was observed.

REFERENCES

1. Hertzberg, A., Bruckner, A., and Bogdanoff, D.W., "The Ram Accelerator: A New Chemical Method of Achieving Ultrahigh Velocities," Proceedings of the 37th Aeroballistic Range Association Meeting, Quebec, Canada, September 9-12, 1986.

2. Hertzberg, A., Bruckner, A.P. and Bogdanoff, D.W., "Ram Accelerator: A New Chemical Method for Accelerating Projectiles to Ultrahigh Velocities," AIAA Journal, Vol. 26, pp. 195-203, 1988.

3. Bruckner, A.P., Bogdanoff, D.W., Knowlen, C. and Hertzberg, A.,"Investigation of Gasdynamic Phenomena Associated with the Ram Accelerator Concept," AIAA Paper 87-1327, June 1987.

4. Knowlen, C., Bruckner, A.P., Bogdanoff, D.W. and Hertzberg, A., "Performance Capabilities of the Ram Accelerator," AIAA Paper 87-2152, July 1987.

5. Hertzberg, A., Bruckner, A.P., Bogdanoff, D.W., and Knowlen, C. "The Ram Accelerator and its Applications: A New Chemical Approach for Reaching Ultrahigh Velocities," Invited Paper, in Shock Tubes and Waves, Proceedings of the 16th International Symposium on Shock Tubes and Waves, Aachen, West Germany, July 26-30, 1987, pp. 117-128.

6. Bruckner, A.P., Knowlen, C., Scott, K.A. and Hertzberg, A., "High Velocity Modes of the Thermally Choked Ram Accelerator," AIAA Paper 88-2925, July 1988.

7. Knowlen, C., Scott, K.A., Bruckner, A.P., and Hertzberg, A., "Recent Developments in Ram Accelerator Technology," Proceedings of the 39th Aeroballistic Range Association Meeting, Albuquerque, NM, October 10-13, 1988.

8. Bruckner, A.P., Knowlen, C., Scott, K.A., Hertzberg, A., and Bogdanoff, D.W., "Operational Characteristics of the Thermally Choked Ram Accelerator," to be published in Journal of Propulsion and Power.

9. Yungster, S., Eberhardt, S. and Bruckner, A.P., "Numerical Simulation of Shock-Induced Combustion Generated by High-Speed Projectiles in Detonable Gas Mixtures," AIAA Paper 89-0673, January 1989.

10. Yungster, S. and Bruckner, A.P., "A Numerical Study of the Ram Accelerator Concept in the Superdetonative Velocity Range," AIAA Paper 89-2677, July 1989.

11. Hertzberg, A., Bruckner, A.P. and Mattick, A.T., "A Chemical Method for Achieving Acceleration of Macroparticles to Ultrahigh Velocities," Final Report, UWAERP/15, Department of Energy Grant No. DE FG06 85ER13382, Aerospace and Energetics Research Program, University of Washington, Seattle, WA, 1987.

12. Bruckner, A.P. and Hertzberg, A., "Ram Accelerator Direct Launch System for Space Cargo," IAF Paper 87-211, 1987.

13. Kaloupis, P. and Bruckner, A.P., "The Ram Accelerator: A Chemically Driven Mass Launcher," AIAA Paper 88-2968, July 1988.

14. Ostrander, M.J., Hyde, M.F., Young, R.D. and Kissinger, R.D., "Standing Oblique Detonation Wave Engine Performance," AIAA Paper 87-2002, June 1987.

15. Pratt, D.T., Humphrey, J.W. and Glenn, D.E., "Morphology of a Standing Oblique Detonation Wave," AIAA Paper 87-1785, June 1987.

16. Hertzberg, A., Bruckner, A.P., Mattick, A.T., and Bogdanoff, D W., "A Chemical Method for Achieving Acceleration of Macroparticles to Ultrahigh Velocities," Progress Report No. 1, DOE Grant No. DE-FG06-85ER13382, Aerospace and Energetics Research Program, University of Washington, Seattle, WA, Feb. 1986.

17. Shapiro, A.H., The Dynamics and Thermodynamics of Compressible Fluid Flow, Vol I, John Wiley and Sons, New York, 1953, pp. 135-137.

18. Dwoyer, D.L., Kutler, P., and Povinelli, L.A., "Retooling CFD for Hypersonic Aircraft," Aerospace America, Vol. 25, Oct. 1987, pp 32-35.

19. Povinelli, L.A., "Advanced Computational Techniques for Hypersonic Propulsion," NASA Technical Memorandum No. 102005, NASA Lewis Research Center, Sept. 1989.

20. Brackett, D.C. and Bogdanoff, D.W., "Computational Investigation of Oblique Detonation Ramjet-in-Tube Concepts," Journal of Propulsion and Power, Vol. 5, May-June 1989, pp. 276-281.

21. Yungster, S., "Numerical Simulation of Shock-Induced Combustion for Application to the Ram Accelerator Concept," Ph.D. Dissertation, Department of Aeronautics \& Astronautics, University of Washington, Oct. 1989.

22. Stull, D.R. and Prophet, H., "JANAF Thermochemical Tables," 2nd. Ed., NSRDS-Report 37, National Bureau of Standards, June 1971.

23. Moretti, G., "A New Technique for the Numerical Analysis of Nonequilibrium Flows," AIAA Journal, Vol. 3, Feb. 1965, pp. 223-229.

24. Evans, J.S. and Schexnayder, C.J., "Influence of Chemical Kinetics and Unmixedness on Burning in Supersonic Hydrogen Flames," AIAA Journal, Vol. 18, Feb. 1980, pp. 188-193.

25. Harten, A., "On a Class of High Resolution Total-Variation-Stable Finite-Difference Schemes," SIAM J. Num. Anal., Vol. 21, 1984, pp. 1-23.

26. Yee, H.C. and Shinn, J.L., "Semi Implicit and Fully Implicit Shock-Capturing Methods for Nonequilibrium Flows," AIAA Journal, Vol. 27, March 1989, pp. 299-307.

27. Ruegg, F.W. and Dorsey, W.W., "A Missile Technique for the Study of Detonation Waves," J. Res. Nat. Bur. Stand., 66C, January 1962, pp. 51-58.

28. Chernyi, G.G., "Supersonic Flow Around Bodies With Detonation and Deflagration Fronts," Astronautica Acta, Vol.13, 1967, pp. 464-480.

29. Behrens, H., Struth, W., and Wecken, F., "Shock-Induced Combustion in the Bow Waves of High-Speed Missiles," Deutsch-Französisches Forschungsinstitut, Rep. 2/66, Saint-Louis, France, 1966.

30. Lehr, H.F., "Experiments on Shock-Induced Combustion," Astronautica Acta, Vol. 17, 1972, pp. 589-597.

31. Prabhu, R., Thareja, R., and Stewart, J., "A Navier-Stokes Solver for High Speed Equilibrium Flows and Application to Blunt Bodies," AIAA Paper 89-0668, Jan. 1989.

APPENDIX A
NUMERICAL FORMULATION

Governing Equations

The analysis presented here is limited at the present time to inviscid flow. For the case of chemically reacting flows, the Euler equations, with the global continuity equation replaced by all the species continuity equations, are used. They can be expressed in the following conservation form for a gas containing n species and in general curvilinear coordinates (ξ, η)

$$\frac{\partial \mathbf{q}}{\partial t} + \frac{\partial \mathbf{F}}{\partial \xi} + \frac{\partial \mathbf{G}}{\partial \eta} + j\mathbf{H} = \mathbf{W} \tag{1}$$

where

$$\mathbf{q} = J^{-1} \begin{bmatrix} \rho_1 \\ \rho_2 \\ \vdots \\ \rho_n \\ \rho u \\ \rho v \\ e \end{bmatrix}, \quad \mathbf{F} = J^{-1} \begin{bmatrix} \rho_1 U \\ \rho_2 U \\ \vdots \\ \rho_n U \\ \rho u U + \xi_x p \\ \rho v U + \xi_y p \\ U(e+p) \end{bmatrix} \tag{2}$$

$$\mathbf{G} = J^{-1} \begin{bmatrix} \rho_1 V \\ \rho_2 V \\ \vdots \\ \rho_n V \\ \rho u V + \eta_x p \\ \rho v V + \eta_y p \\ V(e+p) \end{bmatrix}, \quad \mathbf{H} = \frac{J^{-1}}{y} \begin{bmatrix} \rho_1 v \\ \rho_2 v \\ \vdots \\ \rho_n v \\ \rho u v \\ \rho v^2 \\ v(e+p) \end{bmatrix}$$

$$\mathbf{W} = J^{-1} \begin{bmatrix} w_1 \\ w_2 \\ \vdots \\ w_n \\ 0 \\ 0 \\ 0 \end{bmatrix}$$

The equations describe two-dimensional flow if $j = 0$ and axisymmetric flow if $j = 1$. The variables are the velocity components u and v, the pressure p, the energy per unit

volume e and the density of the ith species ρ_i, with $\rho = \sum_{i=1}^{n} \rho_i$. The terms w_i represent the production of species from chemical reactions and are calculated by standard methods[1]. The variable y is the cylindrical radius. Finally, the grid Jacobian J and the contravariant velocities U and V are defined as follows

$$J^{-1} = x_\xi y_\eta - x_\eta y_\xi$$

$$U = \xi_x u + \xi_y v; \qquad V = \eta_x u + \eta_y v$$

$$\xi_x = J y_\eta; \qquad \xi_y = -J x_\eta$$

$$\eta_x = -J y_\xi; \qquad \eta_y = J x_\xi \tag{3}$$

The terms x_ξ, x_η, etc., are the grid metric terms $\frac{\partial x}{\partial \xi}$, $\frac{\partial x}{\partial \eta}$, etc. The equation of state used is that for a mixture of thermally perfect gases

$$p = \sum_{i=1}^{n} \frac{\rho_i}{M_i} RT \tag{4}$$

where M_i is the molecular weight of the ith species, and R is the universal gas constant. The temperature T, is determined from the definition of the total energy :

$$\sum_{i=1}^{n} c_i \int^T c_{v_i} dT = \frac{e}{\rho} - \frac{1}{2}(u^2 + v^2) - \sum_{i=1}^{n} c_i h_i^0 \tag{5}$$

where $c_i = \frac{\rho_i}{\rho}$, c_{v_i} is the specific heat at constant volume of the ith species, and h_i^0 is the heat of formation for species i. Expressions for the specific heats as a function of temperature are obtained from the JANAF tables[2] and use the following polynomial fit[3]

$$\frac{c_{p_i}}{R} = A_1 + A_2 T + A_3 T^2 + A_4 T^3 + A_5 T^4$$

where c_{p_i} is the specific heat at constant pressure of the ith species, and $A_1, \ldots, A_5$ are constants. It should be mentioned that recent work by Wada et.al.[4] has shown that the assumption of constant specific heat in calculating chemically reacting flows can lead to large errors, because temperatures (on which the reaction rates strongly depend) tend to be overestimated.

Combustion Model

The combustion model used for the present study is the one proposed by Moretti[5] which consists of 6 reacting species H, O, H_2O, OH, O_2, H_2, and an inert species such as Argon or Nitrogen. Eight reactions are assumed to be significant:

$$
\begin{aligned}
H + O_2 &\rightleftharpoons OH + O \\
O + H_2 &\rightleftharpoons OH + H \\
H_2 + OH &\rightleftharpoons H + H_2O \\
2OH &\rightleftharpoons O + H_2O \\
H_2 + X &\rightleftharpoons 2H + X \\
H_2O + X &\rightleftharpoons OH + H + X \\
OH + X &\rightleftharpoons O + H + X \\
O_2 + X &\rightleftharpoons 2O + X
\end{aligned}
$$

The forward and backward reaction rates for the ith reaction, K_{fi} and K_{bi}, are given by expressions of the form

$$K_i = A_i T^{b_i} e^{-C_i/T} \tag{6}$$

The reaction coefficients A_i, b_i, and C_i were taken from Evans and Schexnayder[6], who also analyzed hydrogen/air supersonic flames using the above system of 7 species and 8 reactions. They compared the results with those obtained using a system consisting of 12 species and 25 reactions. The main difference between the 8-reaction and the 25-reaction model was the addition of HO_2, NO, and NO_2. Reactions involving HO_2 (hydroperoxide) are important for low temperature ignition studies. The main conclusions of their study are : 1) Although the 25-reaction model is superior to the 8-reaction model for predicting ignition (due to the presence of more reaction paths for the creation and depletion of free radicals such as H, O, and OH), once ignition occurs, the 8-reaction model results are as good as those from the 25-reaction model; and 2) In a system where external means for ignition are provided or where spontaneous ignition is known to be fast, the 8-reaction system is a good approximation.

More complicated models for hydrogen combustion have also been proposed[7,8]. These include more reaction paths than the 25-reaction model and include also reactions involving H_2O_2 (hydrogen peroxide). For the ram accelerator studies, the inclusion of HO_2 and H_2O_2 could be important at the lower Mach number flight regime, where low temperature ignition occurs. At higher Mach numbers, such species are probably unimportant.

Numerical Method

The equation set describing chemically reacting flows is difficult to solve due to the fact that it is mathematically stiff. Stiffness can be defined as the ratio of the largest to the smallest time scale. In reacting flows, the time scales associated with the chemistry tend to be much smaller than the time scale of fluid motion, sometimes by orders of magnitude. For the equation set being discussed here, the degree of stiffness is determined by the ratio of the characteristic convection time, τ_{conv}, to the characteristic reaction time, τ_{ch}, a parameter known as the Damköhler number

$$Da = \frac{\tau_{conv}}{\tau_{ch}} \tag{7}$$

In general there will be one Damköhler number associated with each chemical reaction.

There are currently two approaches to solving stiff systems of equations. One approach is to uncouple the fluid dynamics equations from the rate equations. Each timestep consists of a fluid dynamics step with frozen chemistry followed by a chemical reaction step (or several small steps) without flow interaction[9,10]. The second approach solves the fully coupled equation set simultaneously. This approach requires an implicit treatment of the chemical source terms which, as shown by Bussing and Murman[11], essentially rescales the equations in time so that all events occur on a similar pseudo-time scale. In the past few years, several algorithms have been developed for calculating nonequilibrium flows based on this approach.[4,11,12,13]

In this paper the fully coupled equation set is solved using a numerical scheme based on a total variation diminishing (TVD) algorithm developed by Yee and Shinn[12], sometimes referred as the "Point Implicit TVD MacCormack" scheme. In generalized coordinates and for a grid spacing $\Delta\xi = \Delta\eta = 1$, it is given by

Predictor:

$$\begin{aligned} \mathbf{D}^n_{j,k}\Delta\mathbf{q}^{(1)}_{j,k} &= -\Delta t(\mathbf{F}^n_{j,k} - \mathbf{F}^n_{j-1,k} + \mathbf{G}^n_{j,k+1} - \mathbf{G}^n_{j,k}) \\ &\quad +\Delta t\mathbf{W}^n_{j,k} \end{aligned} \tag{8}$$

$$\mathbf{q}^{(1)}_{j,k} = \Delta\mathbf{q}^{(1)}_{j,k} + \mathbf{q}^n_{j,k} \tag{9}$$

Corrector:

$$\begin{aligned} \mathbf{D}^1_{j,k}\Delta\mathbf{q}^{(2)}_{j,k} &= \frac{1}{2}[-\Delta\mathbf{q}^{(1)}_{j,k} - \Delta t(\mathbf{F}^{(1)}_{j+1,k} - \mathbf{F}^{(1)}_{j,k} \\ &\quad +\mathbf{G}^{(1)}_{j,k} - \mathbf{G}^{(1)}_{j,k-1})] + \frac{\Delta t}{2}\mathbf{W}^{(1)}_{j,k} \end{aligned} \tag{10}$$

$$\mathbf{q}^{(2)}_{j,k} = \Delta\mathbf{q}^{(2)}_{j,k} + \mathbf{q}^{(1)}_{j,k} \tag{11}$$

$$\begin{aligned}\mathbf{q}^{n+1}_{j,k} = \mathbf{q}^{(2)}_{j,k} &+ [\mathbf{R}^n_{j+\frac{1}{2}}\mathbf{\Phi}^n_{j+\frac{1}{2}} - \mathbf{R}^n_{j-\frac{1}{2}}\mathbf{\Phi}^n_{j-\frac{1}{2}}] \\ &+ [\mathbf{R}^n_{k+\frac{1}{2}}\mathbf{\Phi}^n_{k+\frac{1}{2}} - \mathbf{R}^n_{k-\frac{1}{2}}\mathbf{\Phi}^n_{k-\frac{1}{2}}]\end{aligned} \tag{12}$$

Here $\mathbf{R}_{j\pm\frac{1}{2}}$ denotes the matrix of eigenvectors of the flux Jacobian matrix $\mathbf{A} = \frac{\partial \mathbf{F}}{\partial \mathbf{q}}$ evaluated at some symmetric average of $\mathbf{q}_{j,k}$ and $\mathbf{q}_{j\pm1,k}$, denoted as $\mathbf{q}_{j\pm\frac{1}{2}}$, and $\mathbf{R}_{k\pm\frac{1}{2}}$ denotes the matrix of eigenvectors of the flux Jacobian matrix $\mathbf{B} = \frac{\partial \mathbf{G}}{\partial \mathbf{q}}$ evaluated at $\mathbf{q}_{k\pm\frac{1}{2}}$. The "scaling matrix" $\mathbf{D}$ is given by :

$$\mathbf{D}^n = (\mathbf{I} - \Delta t\theta\frac{\partial \mathbf{W}}{\partial \mathbf{q}}); \quad \mathbf{D}^1 = (\mathbf{I} - \frac{\Delta t}{2}\theta\frac{\partial \mathbf{W}}{\partial \mathbf{q}}) \tag{13}$$

where Δt is the time-step, and θ is a parameter in the range $0 \leq \theta \leq 1$. All our calculations were done with $\theta = 1$ for maximum numerical stability. The elements, $\phi^l_{j+\frac{1}{2}}$, of the dissipation vector $\mathbf{\Phi}_{j+\frac{1}{2}}$ are :

$$\phi^l_{j+\frac{1}{2}} = \frac{1}{2}[\Psi(\nu^l_{j+\frac{1}{2}}) - (\nu^l_{j+\frac{1}{2}})^2][\alpha^l_{j+\frac{1}{2}} - \hat{Q}^l_{j+\frac{1}{2}}] \tag{14}$$

$$\nu^l_{j+\frac{1}{2}} = \Delta t a^l_{j+\frac{1}{2}} \tag{15}$$

$$\alpha_{j+\frac{1}{2}} = \mathbf{R}^{-1}_{j+\frac{1}{2}}(\mathbf{q}_{j+1,k} - \mathbf{q}_{j,k}) \tag{16}$$

Here $a^l_{j+\frac{1}{2}}$ denotes the eigenvalues of $\mathbf{A}$ evaluated at $\mathbf{q}_{j+\frac{1}{2}}$, and $\alpha^l_{j+\frac{1}{2}}$ denotes the elements of the vector $\boldsymbol{\alpha}_{j+\frac{1}{2}}$. The function Ψ is :

$$\Psi(z) = \begin{cases} |z| & |z| \geq \epsilon \\ \frac{(z^2+\epsilon^2)}{2\epsilon} & |z| < \epsilon \end{cases} \qquad .05 \leq \epsilon \leq .2 \tag{17}$$

The "limiter" function $\hat{Q}_{j+\frac{1}{2}}$ used in this study is given by :

$$\hat{Q}^l_{j+\frac{1}{2}} = minmod(\alpha^l_{j-\frac{1}{2}}, \alpha^l_{j+\frac{1}{2}}, \alpha^l_{j+\frac{3}{2}}) \tag{18}$$

Alternative forms of the "limiter" function are given in Ref. 12. The eigenvalues and eigenvectors of the fully coupled chemically reacting equations were obtained by Eberhardt and Brown[14] in Cartesian coordinates. They have been extended to generalized coordinates and used for calculating the vectors $\mathbf{R\Phi}$ appearing in equation (12). The resulting expressions for $\mathbf{R\Phi}$ are given below.

The vector $\alpha_{j+\frac{1}{2}}$ appearing in equation (16) is given by

$$\alpha_{j+\frac{1}{2}} = \begin{bmatrix} \Delta q_1 - c_1 aa \\ \Delta q_2 - c_2 aa \\ \vdots \\ \Delta q_n - c_n aa \\ (-\xi_y^* u + \xi_x^* v) bb + \xi_y^* \Delta q_{n+1} - \xi_x^* \Delta q_{n+2} \\ \frac{1}{2}(aa - \frac{U^*}{a} bb + \frac{\xi_x^*}{a} \Delta q_{n+1} + \frac{\xi_y^*}{a} \Delta q_{n+2}) \\ \frac{1}{2}(aa + \frac{U^*}{a} bb - \frac{\xi_x^*}{a} \Delta q_{n+1} - \frac{\xi_y^*}{a} \Delta q_{n+2}) \end{bmatrix} \tag{19}$$

with

$$\xi_x^* = \frac{\xi_x}{\sqrt{\xi_x^2 + \xi_y^2}} \quad \xi_y^* = \frac{\xi_y}{\sqrt{\xi_x^2 + \xi_y^2}} \tag{20}$$

$$U^* = \frac{U}{\sqrt{\xi_x^2 + \xi_y^2}} \tag{21}$$

$$aa = \frac{1}{a^2}[\sum_{i=1}^{n} P_{\rho_i} \Delta q_i - p_e(u\Delta q_{n+1} + v\Delta q_{n+2} - \Delta q_{n+3})] \tag{22}$$

$$bb = \sum_{i=1}^{n} \Delta q_i, \qquad \Delta q = \frac{q_{j+1,k} J_{j+1,k} - q_{j,k} J_{j,k}}{0.5(J_{j+1,k} + J_{j,k})} \tag{23}$$

And it is understood that all the terms are evaluated at $(j + \frac{1}{2}, k)$. The vector $\mathbf{R\Phi}$ which appears in equation (12) is given by

$$\mathbf{R}_{j+\frac{1}{2}} \mathbf{\Phi}_{j+\frac{1}{2}} = \begin{bmatrix} \phi^1 + c_1 K_1 \\ \phi^2 + c_2 K_1 \\ \vdots \\ \phi^n + c_n K_1 \\ uK_2 + \xi_y^* \phi^{n+1} + \xi_x^* a K_3 \\ vK_2 - \xi_x^* \phi^{n+1} + \xi_y^* a K_3 \\ HK_2 - \frac{1}{p_e} \sum_{i=1}^{n} a_i^2 \phi^i + aU^* K_3 \\ +(\xi_y^* u - \xi_x^* v)\phi^{n+1} \end{bmatrix} \tag{24}$$

with

$$K_1 = \phi^{n+2} + \phi^{n+3}, \quad K_2 = \sum_{i=1}^{n+3} \phi^i$$

$$K_3 = \phi^{n+2} - \phi^{n+3}$$

where the elements, ϕ^l, of the dissipation vector are given by equation (14). The eigenvalues, $a^l_{j+\frac{1}{2}}$, are given by

$$(a^1_{j+\frac{1}{2}}, \ldots, a^{n+3}_{j+\frac{1}{2}}) = (U, \ldots, U, U, U + a\sqrt{\xi_x^2 + \xi_y^2}, U - a\sqrt{\xi_x^2 + \xi_y^2})_{j+\frac{1}{2},k} \tag{25}$$

The frozen sound speed a is

$$a^2 = p_\rho + p_e(H - u^2 - v^2) \tag{26}$$

with H being the total enthalpy per unit mass. Also the following relations are needed

$$p_{\rho_i} = \frac{RT}{M_i}(1 - p_e) + p_e(\frac{u^2 + v^2}{2} - \int^T c_{p_i} dT - h_i^0) \tag{27}$$

$$p_e = \sum_{i=1}^{n} \frac{c_i}{M_i} \frac{R}{c_v} \tag{28}$$

$$p_\rho = \sum_{i=1}^{n} c_i p_{\rho_i} \tag{29}$$

Similar expresions for $\alpha_{k+\frac{1}{2}}$ and $\mathbf{R}_{k+\frac{1}{2}}\mathbf{\Phi}_{k+\frac{1}{2}}$ are obtained by replacing ξ_x by η_x, ξ_y by η_y and U by V.

This scheme is second-order accurate in space and is suitable for steady-state calculations.

References

1. Vincenti, W.G. and Kruger, C.H., *Introduction to Physical Gas Dynamics*, Wiley, New York, 1985, Chap. VII.

2. Stull, D.R. and Prophet, H., "JANAF Thermochemical Tables, 2nd. Ed.," NSRDS-Report 37, National Bureau of Standards, June 1971.

3. Esch, D.D., Siripong, A. and Pike, R. W., "A technical Report on Thermodynamic Properties In Polynomial Form For Carbon, Hydrogen, Nitrogen and Oxygen Systems From 300 to 15000°K," NASA-RFL-TR-70-3, Nov. 1970.

4. Wada, Y., Kubota, H., Ogawa, S. and Ishiguro, T., "A Diagonalizing Formulation of General Real Gas-Dynamic Matrices With a New Class of TVD Schemes," AIAA Paper 88-3596-CP, July 1988.

5. Moretti, G., "A New Technique for the Numerical Analysis of Nonequilibrium Flows," *AIAA Journal*, vol. 3, Feb. 1965, pp. 223-229.

6. Evans, J.S. and Schexnayder, C.J., "Influence of Chemical Kinetics and Unmixedness on Burning in Supersonic Hydrogen Flames," *AIAA Journal*, vol. 18, Feb. 1980, pp. 188-193.

7. Jachimowski, C.J.,"An Analytical Study of the Hydrogen-Air Reaction Mechanism with Application to Scramjet Combustion," NASA TP 2791, Feb. 1988.

8. Oran, E., Young, T. and Boris, J., "Application of Time-Dependent Numerical Methods to the Description of Reactive Shocks," *Proc. 17th Int. Symp. on Combustion,* The Combustion Institute, Pittsburg, Pa., 1978.

9. Bogdanoff, D.W. and Brackett, D.C., "A Computational Fluid Dynamics Code for the Investigation of Ramjet-in-Tube Concepts," AIAA Paper 87-1978, June 1987.

10. Cambier, J.L., Adelman, H. and Menees, G.P., "Numerical Simulations of an Oblique Detonation Wave Engine," AIAA Paper 88-0063, Jan. 1988.

11. Bussing, T.R.A. and Murman, E.M.,"Finite-Volume Method for the Calculation of Compressible Chemically Reacting Flows," *AIAA Journal*, vol. 26, Sept. 1988, pp. 1070-1078.

12. Yee, H.C. and Shinn, J.L., "Semi Implicit and Fully Implicit Shock-Capturing Methods for Nonequilibrium Flows," *AIAA Journal,* vol. 27, March 1989, pp. 299-307.

13. Candler, G.V. and MacCormack, R.W., "The Computation of Hypersonic Ionized Flows in Chemical Thermal Nonequilibrium," AIAA Paper 88-0511, Jan. 1988.

14. Eberhardt, S. and Brown K "A Shock Capturing Technique for Hypersonic, Chemically Relaxing Flows," AIAA Paper 86-0231, June 1986.

APPENDIX B

PUBLICATIONS SUPPORTED BY CONTRACT

1. Yungster, S., Eberhardt, S., and Bruckner, A.P., "Numerical Simulation of Shock-Induced Combustion Generated by High Speed Projectiles in Detonable Gas Mixtures," AIAA Paper No. 89-0673, AIAA 27th Aerospace Sciences Meeting, Reno, NV, January 9-12, 1989. (Also accepted for publication in AIAA Journal)

2. Kull, A.E., Burnham, E.A., Knowlen, C., Bruckner, A.P., and Hertzberg, A., "Experimental Studies of Superdetonative Ram Accelerator Modes," AIAA Paper No. 89-2632, AIAA/ASME/SAE/ASEE 25th Joint Propulsion Conference, Monterey, CA, July 10-12, 1989.

3. Yungster, S. and Bruckner, A., "A Numerical Study of the Ram Accelerator Concept in the Superdetonative Velocity Range,", AIAA Paper No. 89-2677, AIAA/ASME/SAE/ASEE 25th Joint Propulsion Conference, Monterey, CA, July 10-12, 1989.

4. Hertzberg, A., "Thermodynamics of the Ram Accelerator," Paul Vieille Memorial Lecture, 17th International Symposium on Shock Tubes and Waves, Bethlehem, PA, July 17-21, 1989.

5. Bruckner, A.P., Hertzberg, A., Kull, A.E., Burnham, E.A., Knowlen,C., and Yungster, S., "High Velocity Modes of the Ram Accelerator," Proceedings of the 40th Meeting of the Aeroballistic Range Association, Paris France, September 25-28, 1989.